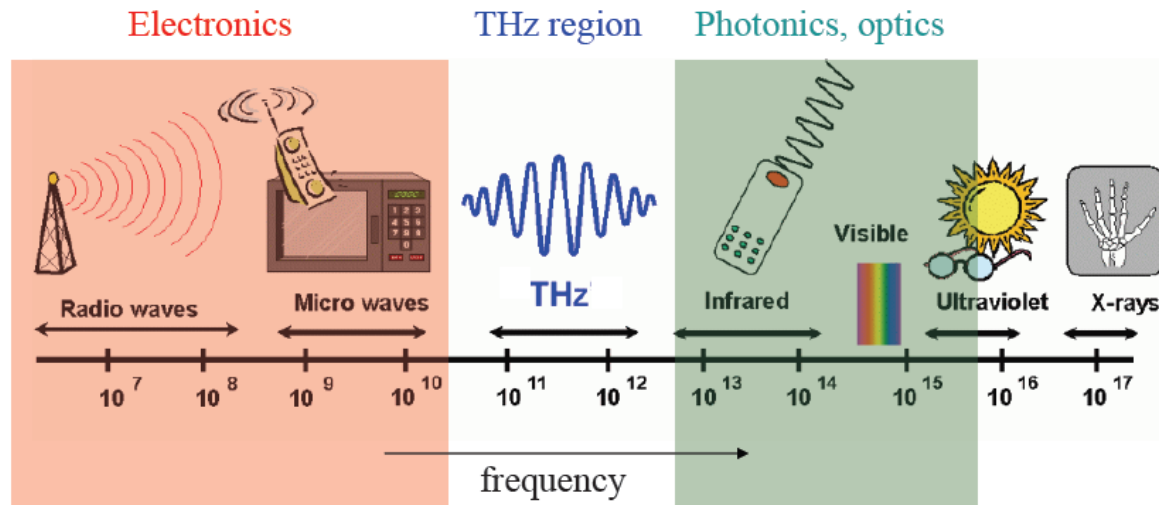



New sources of THz radiation

A. Potylitsyn

Tomsk Polytechnic University



typical:  $\lambda/c = 10^{-12} \text{ s} = 1 \text{ ps}$
 $\lambda = 0.3 \text{ mm}$

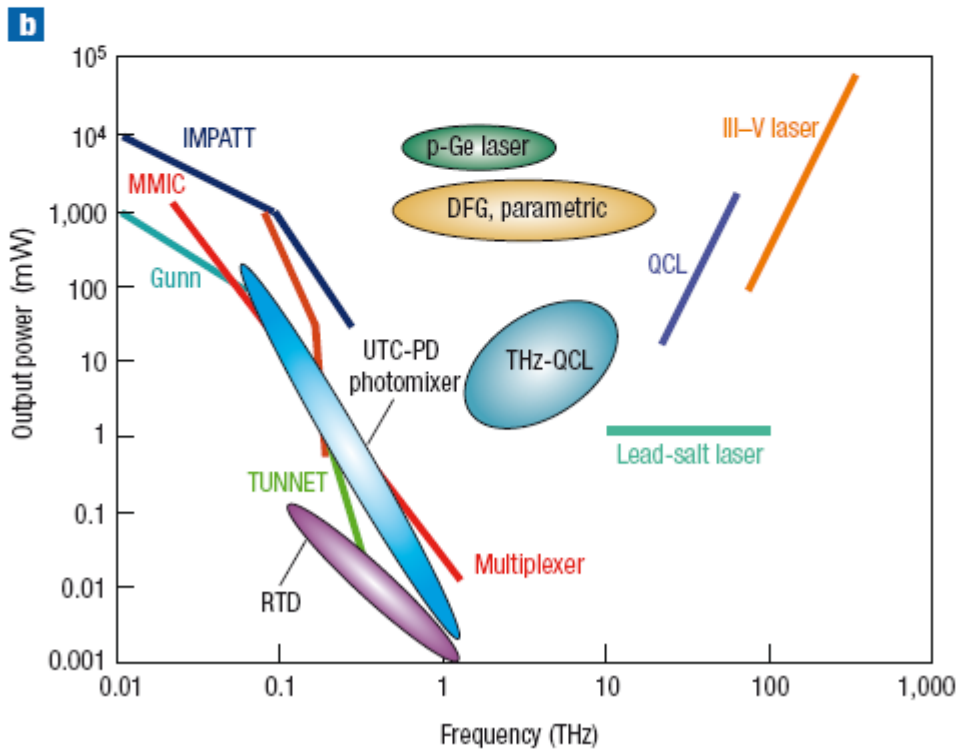
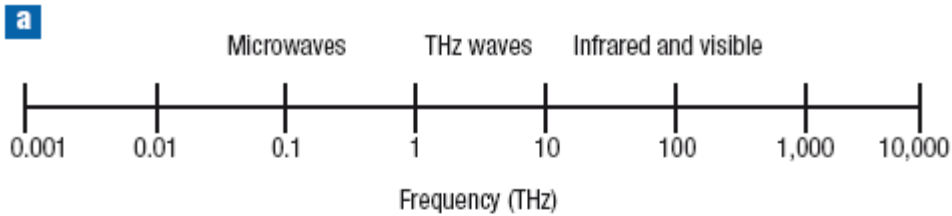
The terahertz (1 THz = 10^{12} Hz) spectral range roughly extends from 100 GHz to 10 THz, which positions it in between electronics and photonics, see Fig. 1.

Since the advent of ultrafast lasers in the late 1980's the THz spectral range has opened up to researchers, leading to an enormous increase in studies performed at THz frequencies.

Since THz radiation is non-ionizing, it is expected to have applications in medical imaging as well.

Electrons in highly-excited atomic Rydberg states orbit at THz frequencies; small molecules rotate at THz frequencies; biologically important collective modes of proteins vibrate at THz frequencies; electrons in semiconductor nanostructures resonate at THz frequencies.

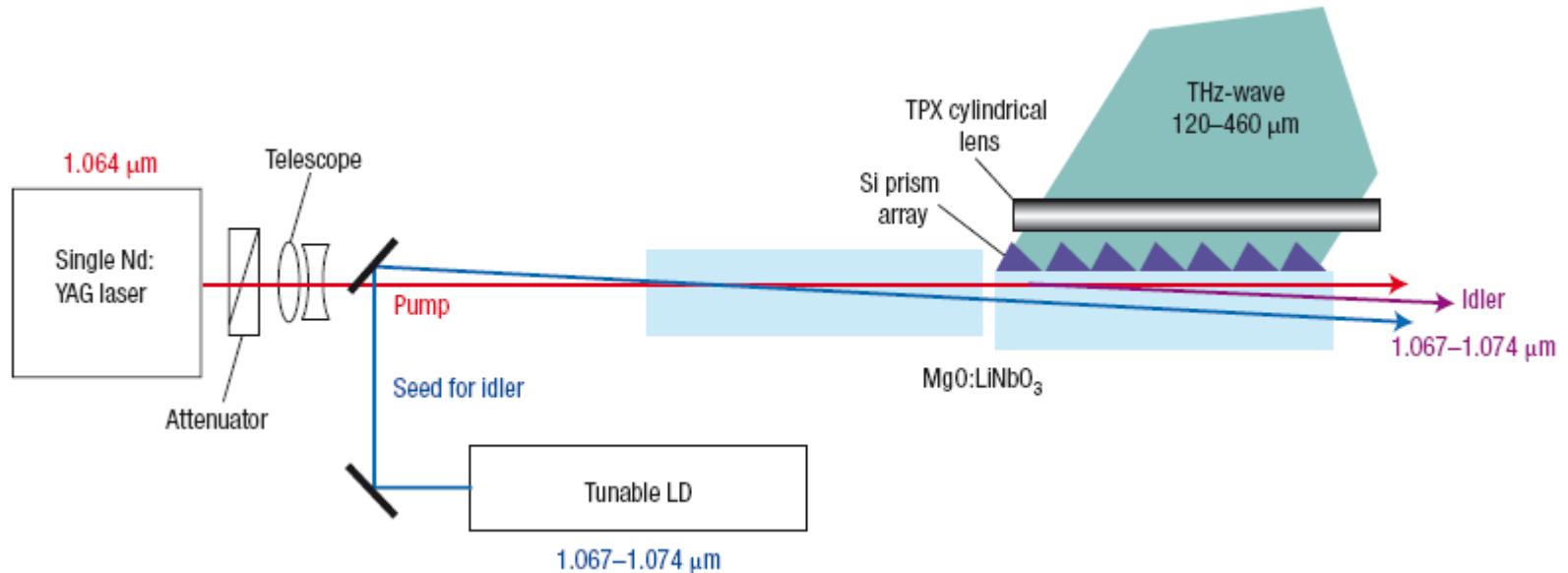
Powerful THz sources are very desirable, simply from signal-to-noise point of view. In addition, they could prove valuable tools to investigate matter in the non-linear regime.



Welcome to the terahertz region. **a, A schematic showing the THz region** within the electromagnetic spectrum. Although there is no strict definition of what qualify as THz waves it seems reasonable to consider the region between 100 GHz and 30 THz. **b, THz-emission power as a function of frequency. Solid lines are for the conventional THz sources; IMPATT diode stands for impact ionization avalanche transit-time diode, MMIC stands for microwave monolithic integrated circuit, TUNNET stands for tunnel injection transit time and the multiplexer is an SBD frequency multiplier. Ovals denote recent THz sources. The values of the last two are indicated by peak power; others are by c.w. power.** (Masayoshi Tonouchi, *Nature Photonics*, 1 (2007) 97-105)

Femtosecond laser are used for THz radiation generation

(Masayoshi Tonouchi , nature photonics, p. 99)



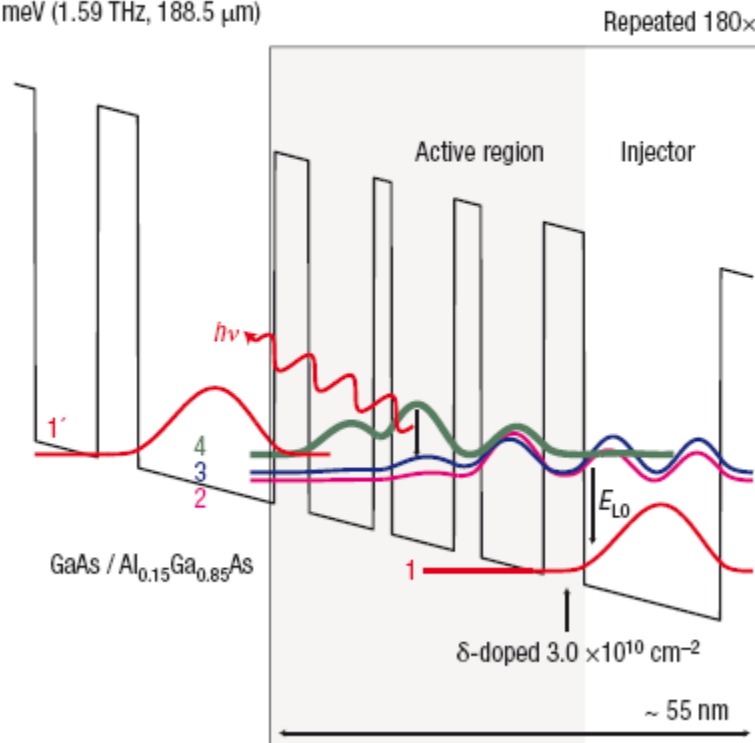
Typical design of a solid-state source of tunable THz waves based on an injection-seeded THz-wave parametric generator. (IS-TPG). The pump laser was a single longitudinal mode Q-switched Nd:YAG laser (1.064 μm), and the seed for the idler was a c.w. Yb-fibre laser (1.070 μm) or tunable laser diode (1.067–1.074 μm). Generated THz waves in LiNbO₃ are coupled with a silicon prism array and emit into free space through a TPX (poly-methyl-1-pentene) cylindrical lens.

Lasing frequencies as low as 1.59 THz have been achieved in a resonant-phonon-assisted THz-quantum cascade laser.

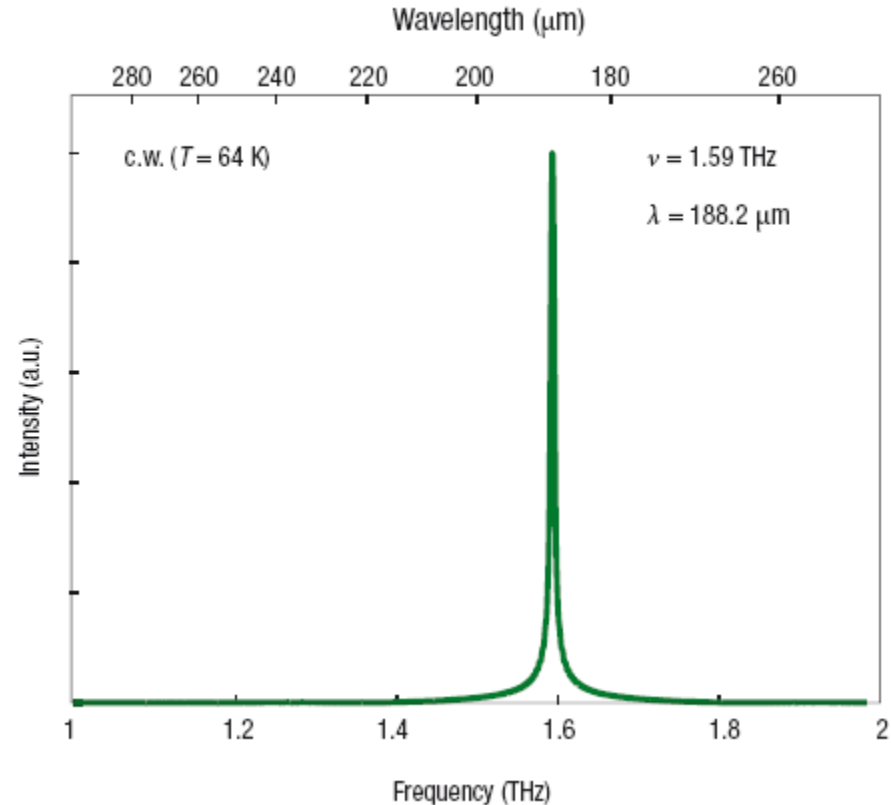
a

44 mV per module (7.8 kV cm^{-1})

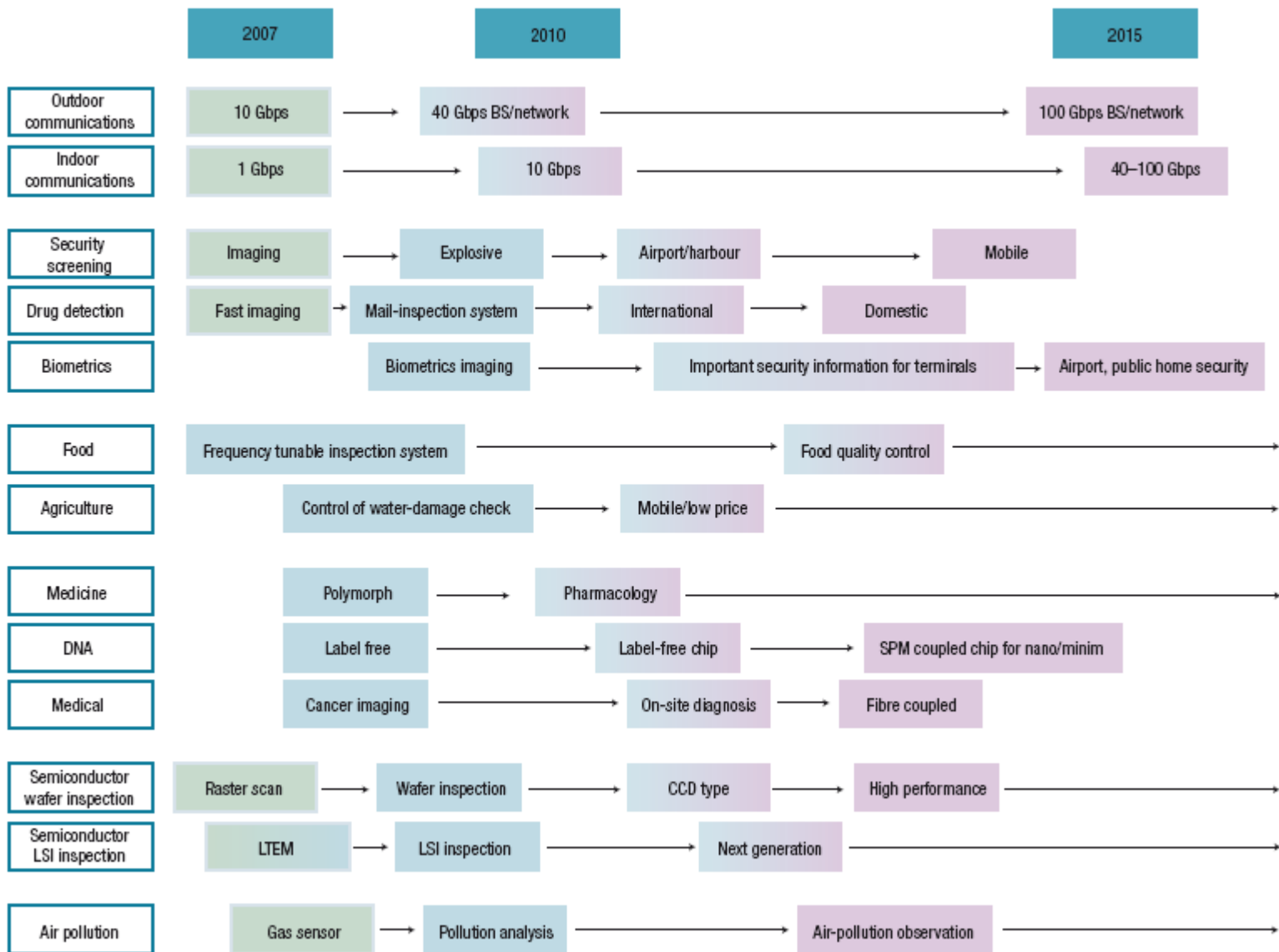
$h\nu = 6.58 \text{ meV}$ (1.59 THz, $188.5 \text{ }\mu\text{m}$)



b



Semiconductor source of THz waves based on a QCL design. **a, Conduction band profile of a GaAs–AlGaAs quantum-well-based QCL. Terahertz waves are generated** in the active region by electron relaxation from band 4 (green) to band 3 (blue), followed by the relaxation from band 3 to band 1 (red) by means of longitudinal-optical (LO) phonon mode scattering. h is Planck's constant and ν is the frequency. **b, c.w.-emission spectrum above threshold at a temperature of 64 K. The emission frequency** corresponds to 1.59 THz, which is the shortest QCL lasing frequency at present.



Expected roadmap for some THz applications. BS/network stands for broadcast station, fixed wireless-access network, storage station; SPM stands for scanning probe microscopy; and nano/minim stands for nanoscale and/or ultratrace amounts of DNA. (Masayoshi Tonouchi, *nature photonics*, p. 104)

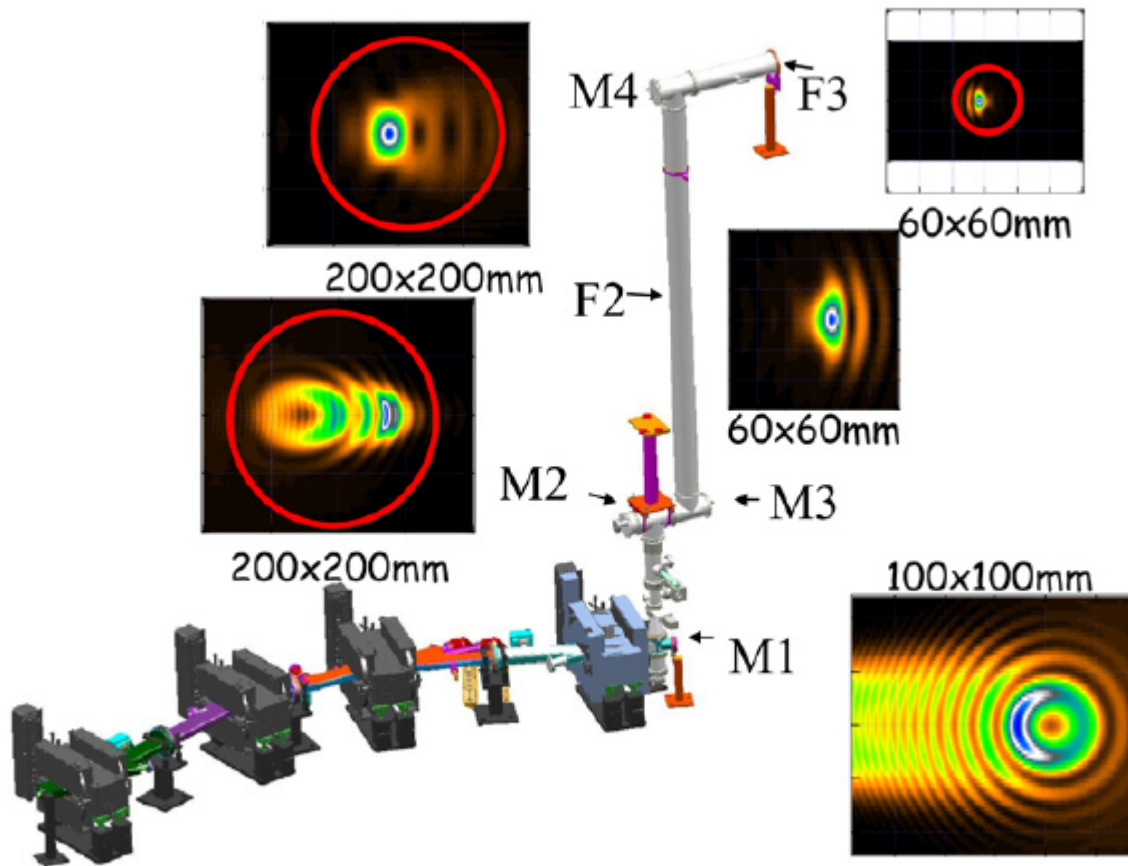
Generation of THz radiation by short electron bunches

Coherent radiation mechanisms:

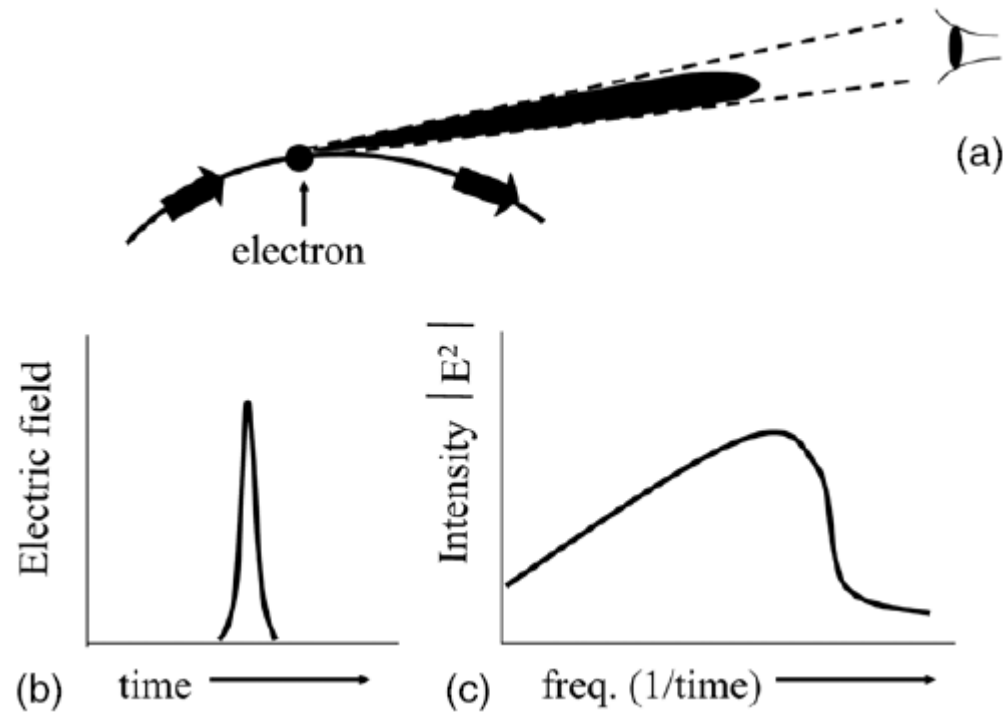
- Synchrotron radiation
- Transition radiation
- Diffraction radiation
- Cherenkov radiation
- Smith- Purcell radiation

Synchrotron radiaton

(Gwyn P Williams, Rep. Prog. Phys. 69 (2006) 301–326)



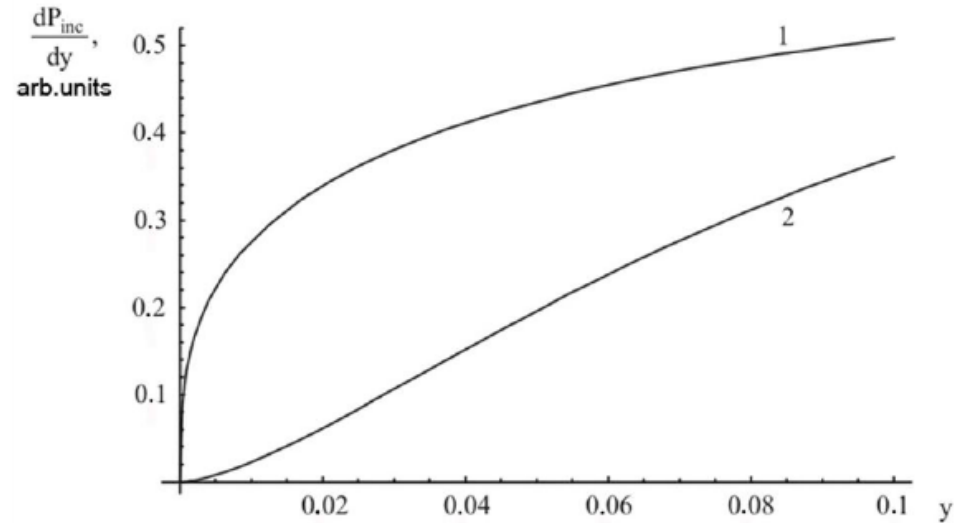
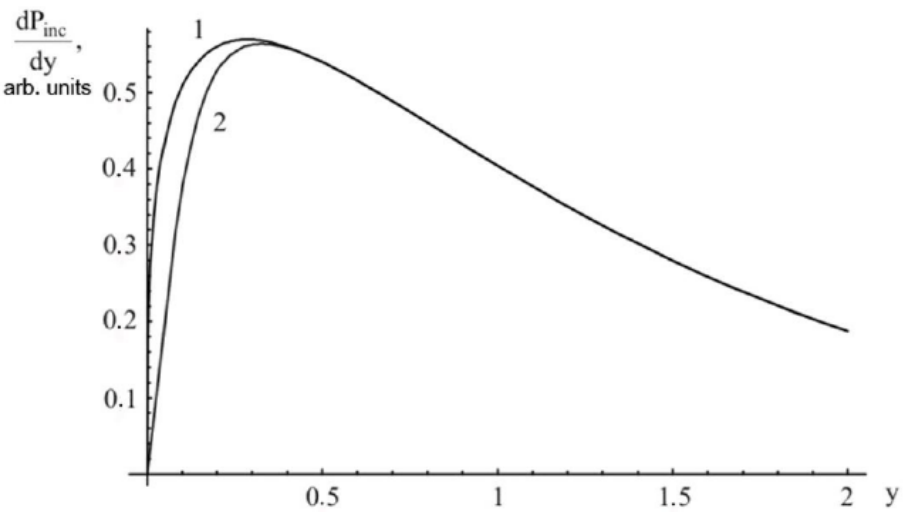
Schematic of the Jefferson Lab high power THz beamline, showing in particular calculations of the emitted and propagating field using the SRW code. The dimensions of the screens are shown, while the circles represent the sizes of the optical components.



$$\Delta t = 2 \frac{2\pi R}{c\gamma}, \quad \omega_c = \frac{3}{2} \frac{\gamma^3 c}{R}$$

Schematic showing the physics of synchrotron radiation generation. An observer of an electron travelling in an arc in (a), 'sees' an electric field pulse (b), whose power spectrum is given by the Fourier transform (c).

SR into a finite aperture

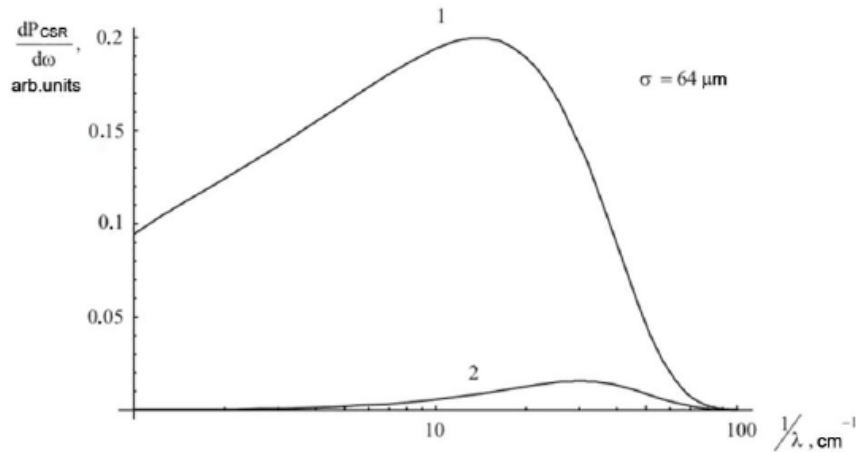


Spectral distribution of the power of incoherent synchrotron radiation in (line 1) the total cone and (line 2) the angular cone $\vartheta = 2.4 \cdot \gamma^{-1}$ with respect to the instantaneous velocity of the electron.

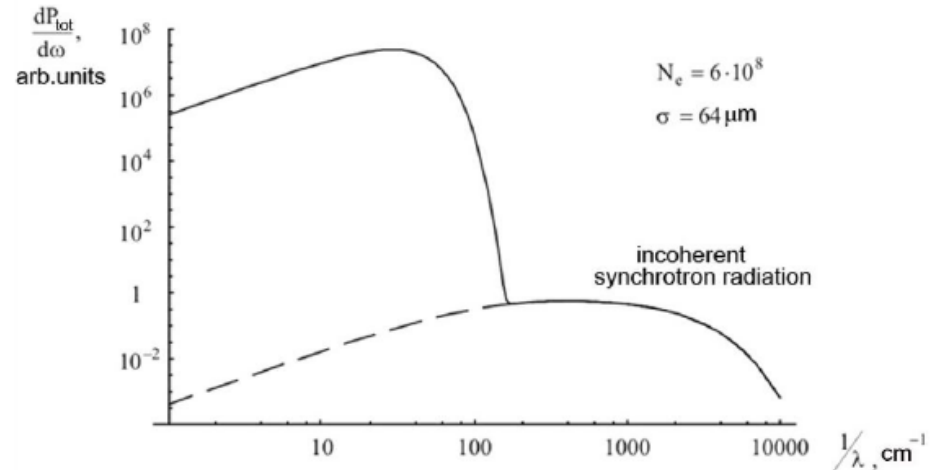
$$\frac{dP_{inc}}{dy} = P_0 C_{inc} y, \quad y = \omega / \omega_c$$

Coherent SR into a finite aperture

(A. P. Potylitsyn, J. Phys. G: Nucl. Part. Phys. 37 (2010) 115106)



Intensity of coherent synchrotron radiation for $\sigma = 64 \mu\text{m}$ in the (line 1) total cone and (line 2) angular cone $\theta \leq 2.4\gamma^{-1}$.



Total spectrum of synchrotron radiation in the angular cone $\theta \leq 2.4\gamma^{-1}$ of an electron bunch with $N_e = 6 \cdot 10^8$ and $\sigma = 64 \mu\text{m}$. The upper and lower lines are coherent and incoherent radiations, respectively.

$$P_{coh}^{SR} = 0.55 \cdot N_e \frac{\alpha \hbar c^2}{R^2} \left(\frac{R}{\sigma} \right)^{\frac{4}{3}}, \quad \gamma \ll N_e^{\frac{1}{4}} \left(\frac{R}{\sigma} \right)^{\frac{1}{3}}$$

$$\gamma \ll 4400 \text{ for } N_e = 6 \cdot 10^8, \quad R = 1\text{m}, \quad \sigma = 64 \mu\text{m}$$

No dependence on Lorentz factor.

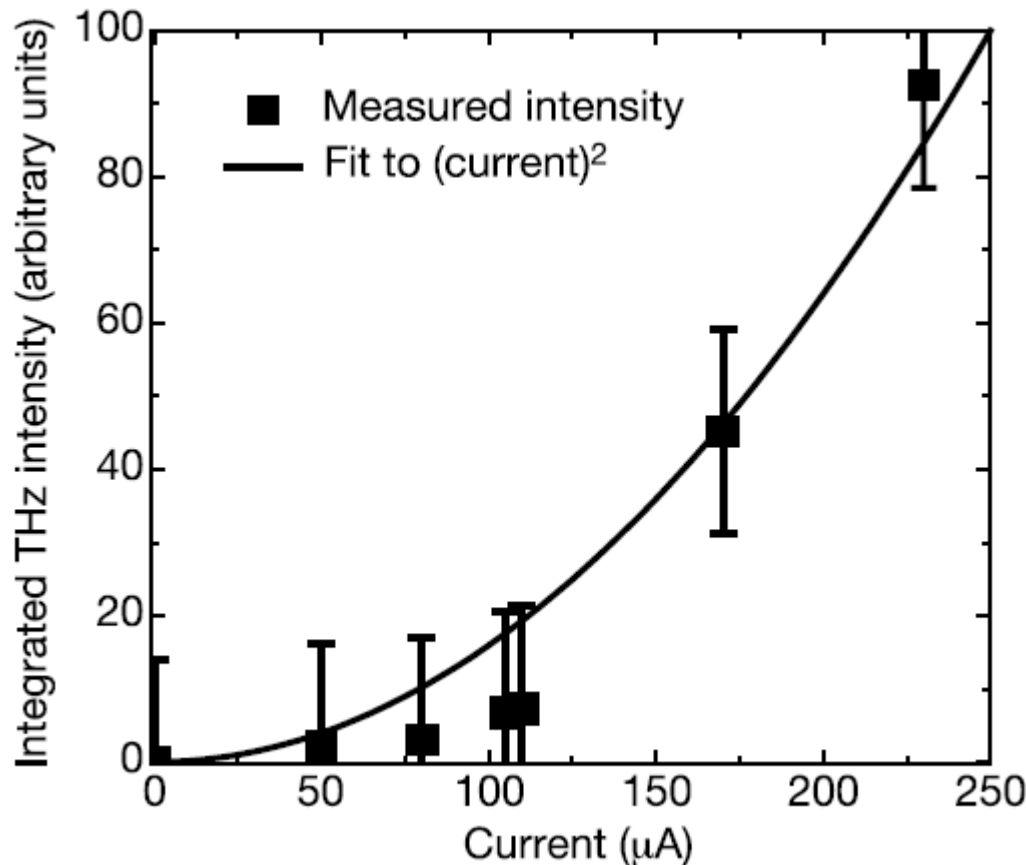
$$W_{coh}^{SR} = P_{coh}^{SR} \cdot \Delta t$$

Experiment

(G. L. Carr, Nature 420, 153 (2002))

$$N_e = 6 \cdot 10^8, \quad \gamma = 80, \quad t_{\max} = 2.4, \quad R = 1m, \quad \sigma = 64 \mu m, \quad l_B = 2.36 \sigma.$$

The average power is nearly 20 watts, several orders of magnitude higher than any existing source



$$\Delta t \approx 5 \cdot 10^{-10} \text{ sec}$$

$$P_{coh} \approx 2 \cdot 10^{-6} \text{ W}$$

$$W_{csr} = P_{coh} \cdot \Delta t = 6 \cdot 10^3 \text{ eV}$$

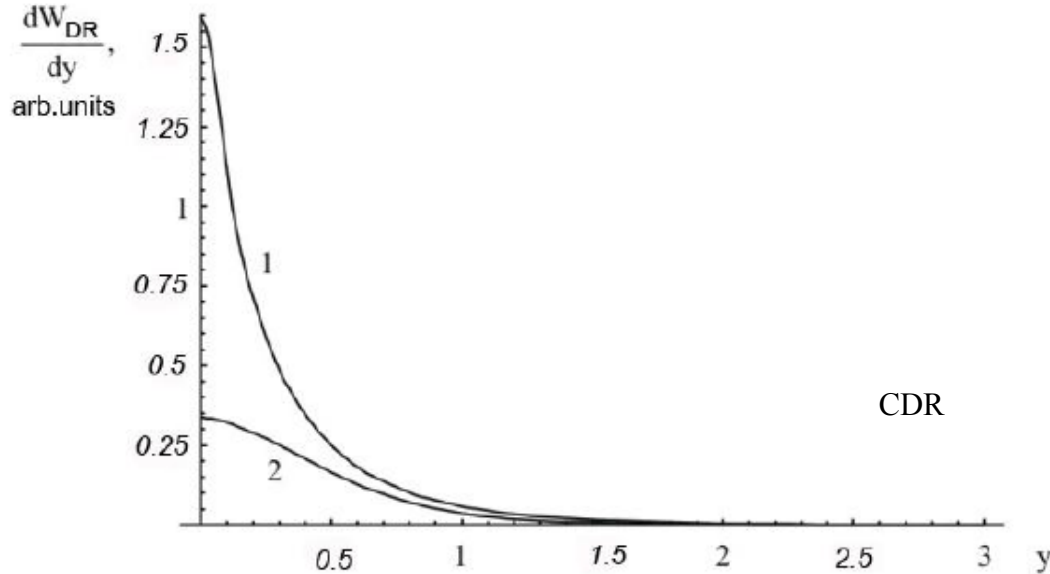
$$\bar{P} \approx W_{CSR} \cdot N_e \cdot f_0 \approx 20 \text{ W}$$

$$(f_0 = 37.4 \text{ MHz})$$

Coherent Diffraction Radiation

A bunch with length $\sim \sigma$ passes through a circular hole with radius ρ .

DR from a single electron :

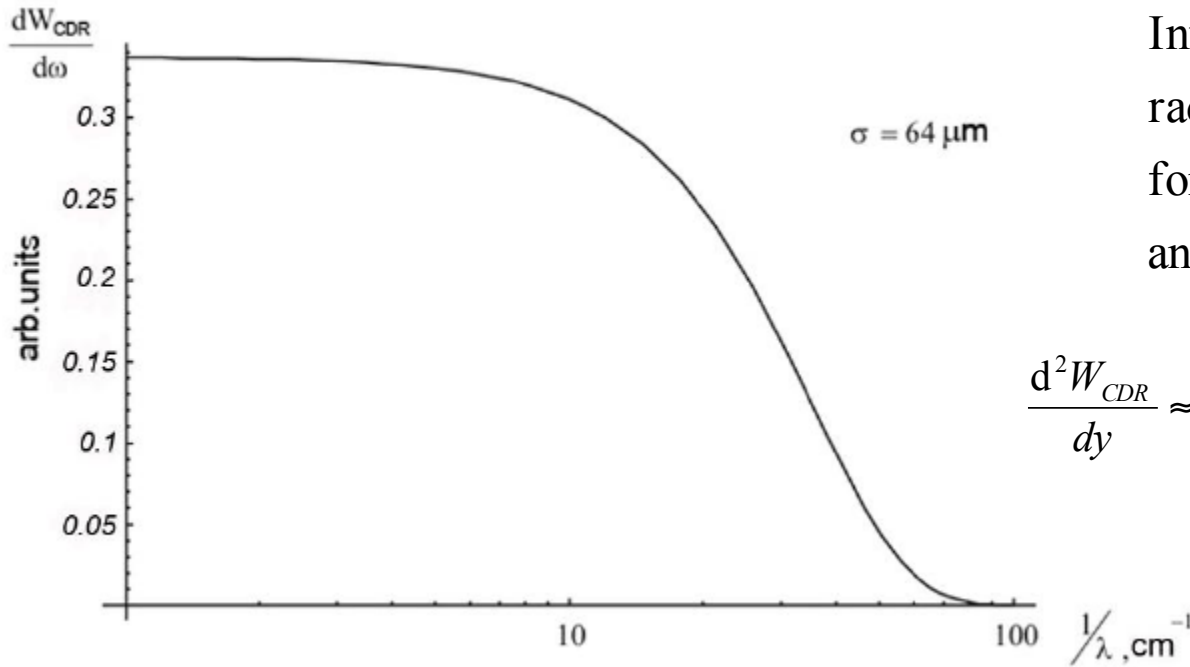


Spectral distribution of the intensity of diffraction radiation generated by a relativistic charge moving through a hole of radius $\rho = 1$ mm (lines 1 and 2) correspond to radiation in the total cone and in the angular cone $t = 2.4$, respectively.

$$t = \gamma\theta, \quad y = \omega/\omega_{DR}, \quad \omega_{DR} = \frac{c\gamma}{\rho}.$$

$$\frac{d^2W_{DR}}{dydt} = \frac{4\alpha\hbar}{\pi} \omega_c \frac{t^2}{(1+t^2)^2} [yK_1(y)J_0(yt)]^2, \quad W_{FDR} \approx \frac{1}{2} \alpha\hbar c \frac{\gamma}{\rho}$$

CDR spectrum is almost const for $y \ll 1$ ($\frac{dW}{dy} = C_{DR}$)



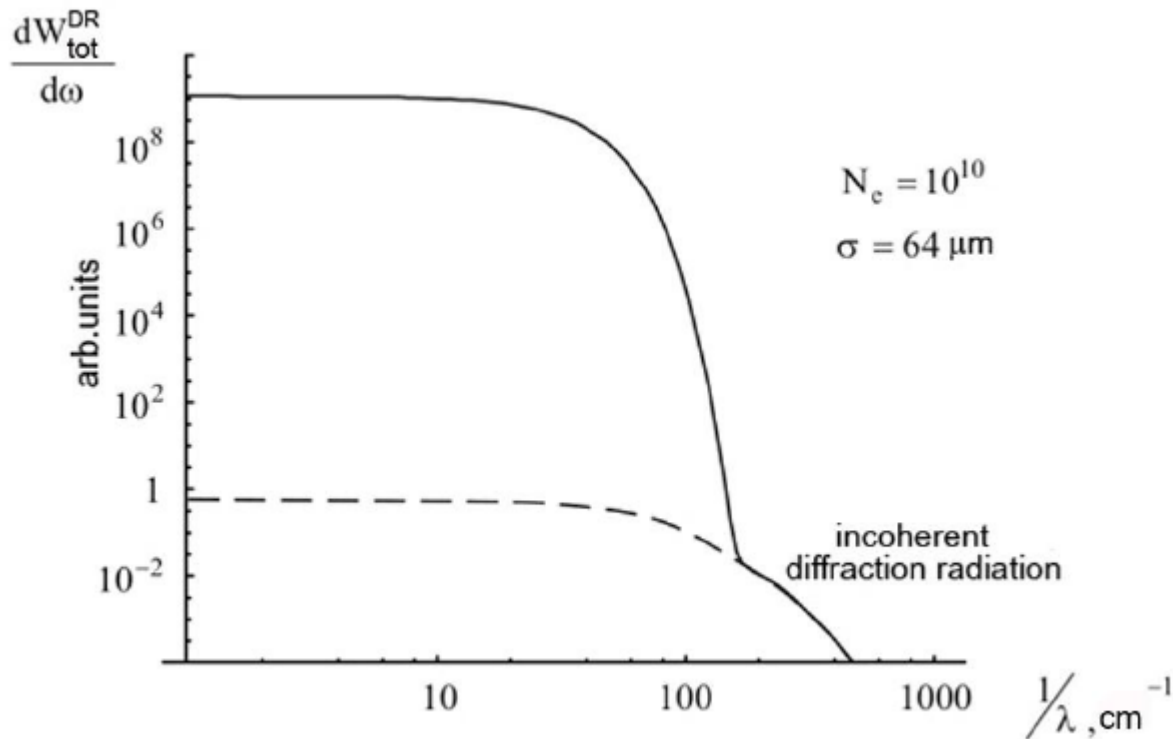
Intensity of coherent diffraction radiation versus the wavenumber for the same parameters as in and $\zeta = 64 \mu\text{m}$.

$$\frac{d^2 W_{CDR}}{dy} \approx N_e \frac{4\alpha\hbar}{\pi} \omega_{DR} C_{DR} \exp\left[-\frac{1}{2}\left(\frac{\gamma}{\rho}\right)^2 \sigma^2 y^2\right]$$

$$W_{CDR} \approx N_e \frac{4\alpha\hbar c}{\sqrt{2\pi}} C_{DR} / \sigma$$

No dependence on a hole radius (if $2\pi c/\sigma \ll c\gamma/\rho$) !

For the same parameters as before ($\sigma = 64 \mu\text{m}$, $\theta = 2.4 \gamma^{-1}$) the spectrum of CDR



$$W_{CDR} = 6 \cdot 10^4 \frac{\text{eV}}{e^-}$$

With taking into account an aperture the same order of radiated energy as for CSR!

$$\bar{P}_{CDR} \approx \bar{W}_{CDR} \cdot N_e \cdot f_0 \sim 10^3 \text{ eV} \cdot 10^9 \cdot 10 \text{ kHz} \sim 10 \text{ mW}$$

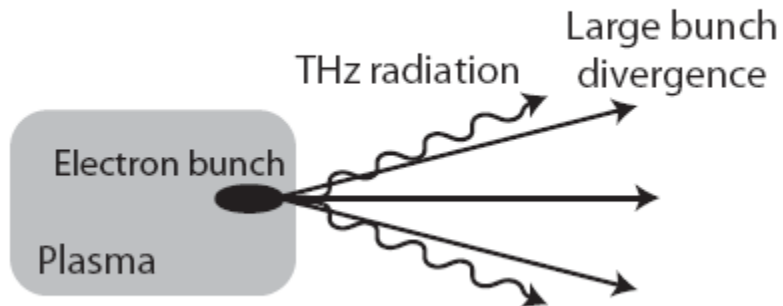
LWFA electron bunches

C.O.R. Geddes et al., PRL 95, 145002 (2005)

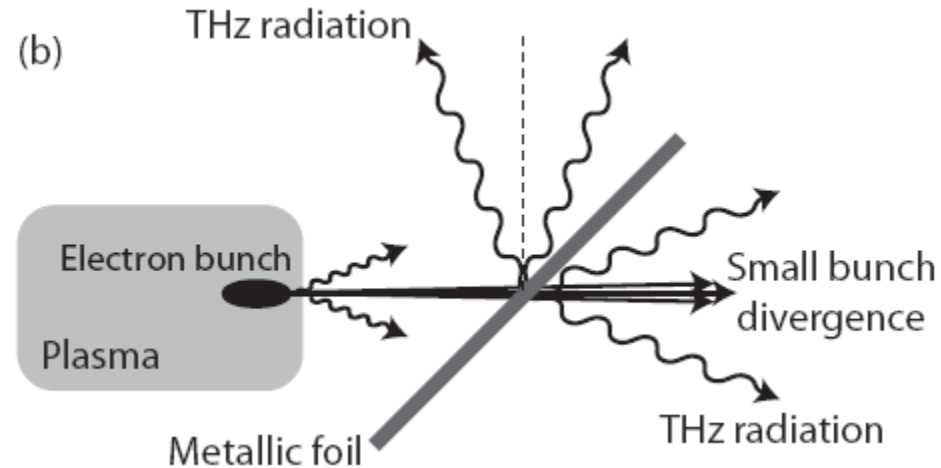
$\lambda_p \sim 5 \div 10 \mu m$, total bunch length $\sim 5 \div 30 \mu m$, transversal size $\sim 5 \div 10 \mu m$

$$\rho(E) \sim \exp\left(-\frac{E}{E_B}\right), \quad E_B = 4.2 \text{ MeV}$$

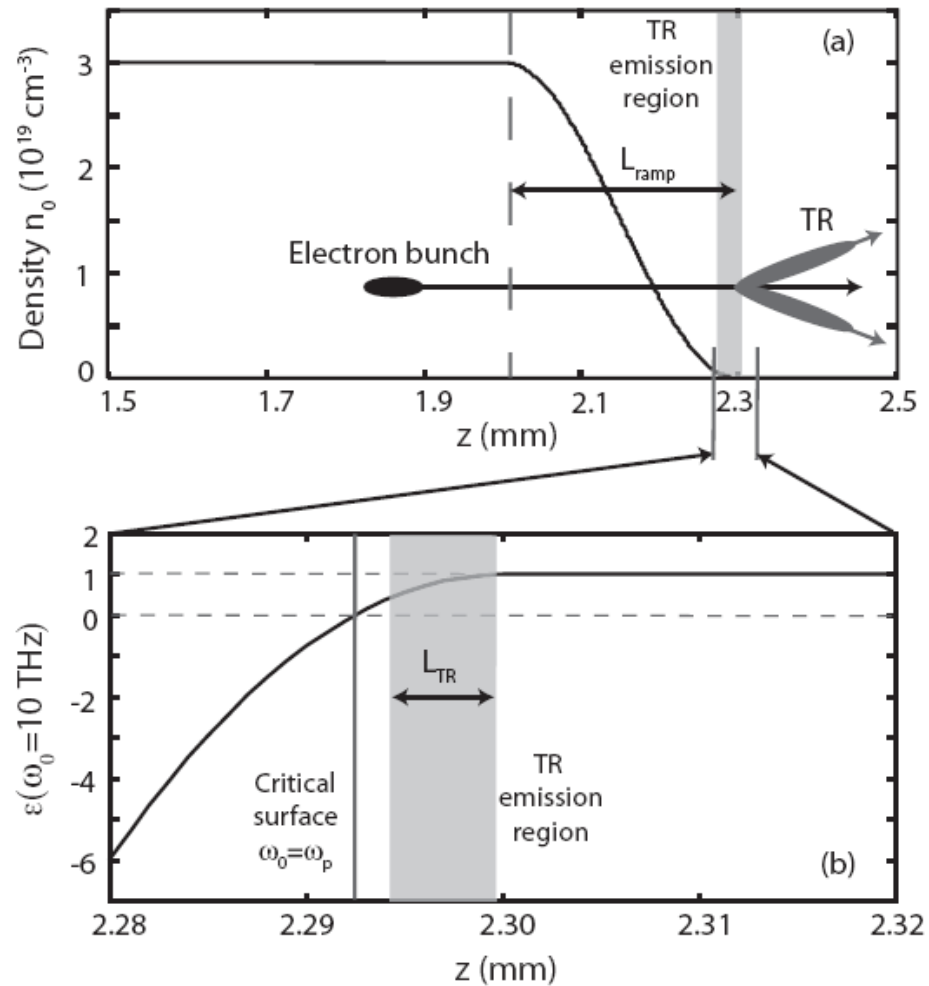
(a)



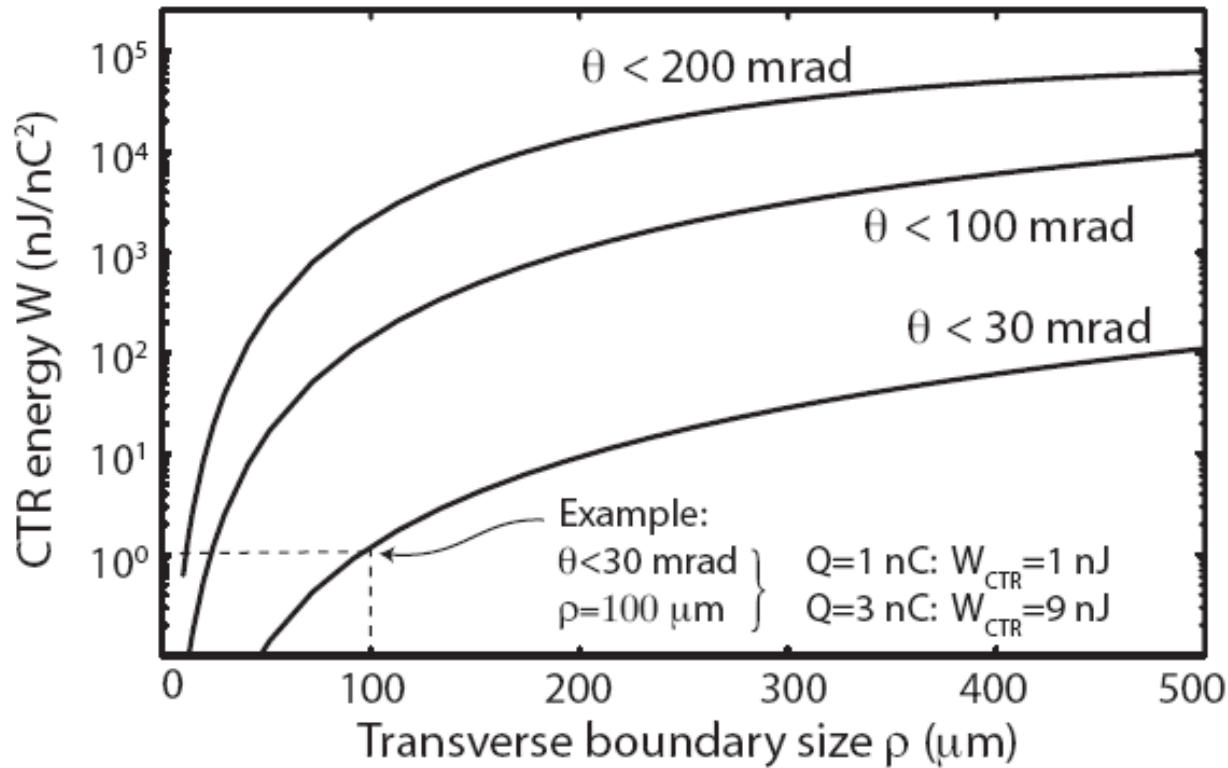
(b)



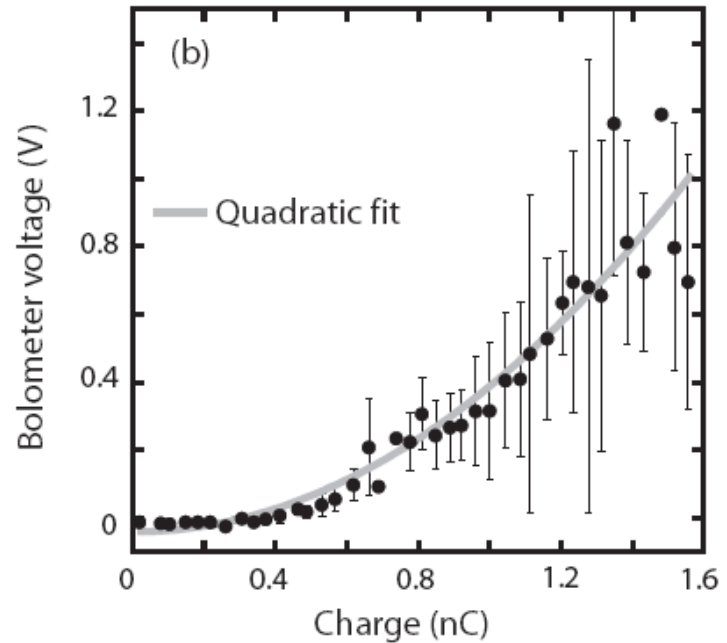
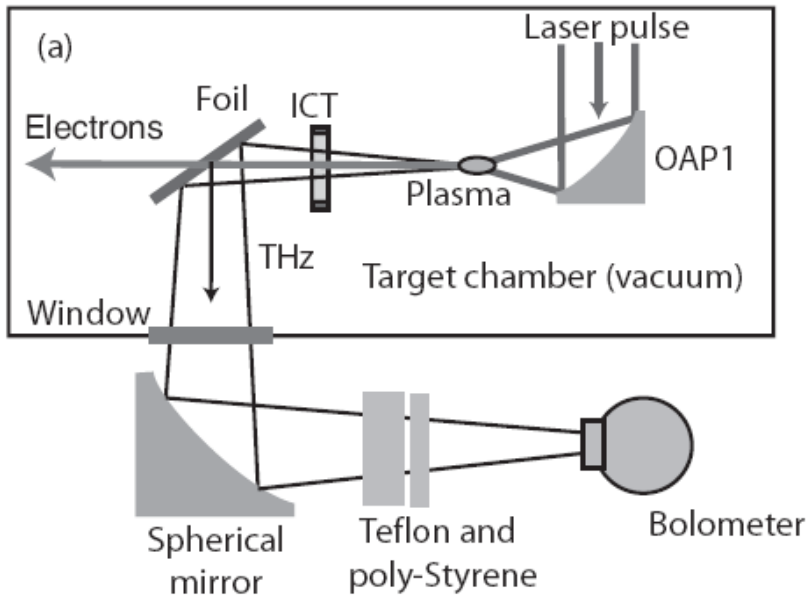
(a) If the LWFA-produced electron bunch has a large energy spread and large bunch divergence, one has to rely on the plasma-vacuum interface for THz emission. (b) However, channel-guided LWFA-produced bunches have a percent-level energy spread, and a divergence of < 3 mrad. For this reason, the spatial and temporal coherence at the location of a metallic foil is still conserved, and intense THz radiation can be collected.



(a) Longitudinal plasma density profile $n_0(z)$. (b) The spatially varying dielectric constant (z, ω_0) , for radiation at frequency $\omega_0 = 10 \text{ THz}$. The electron bunch is propagating from left to right.

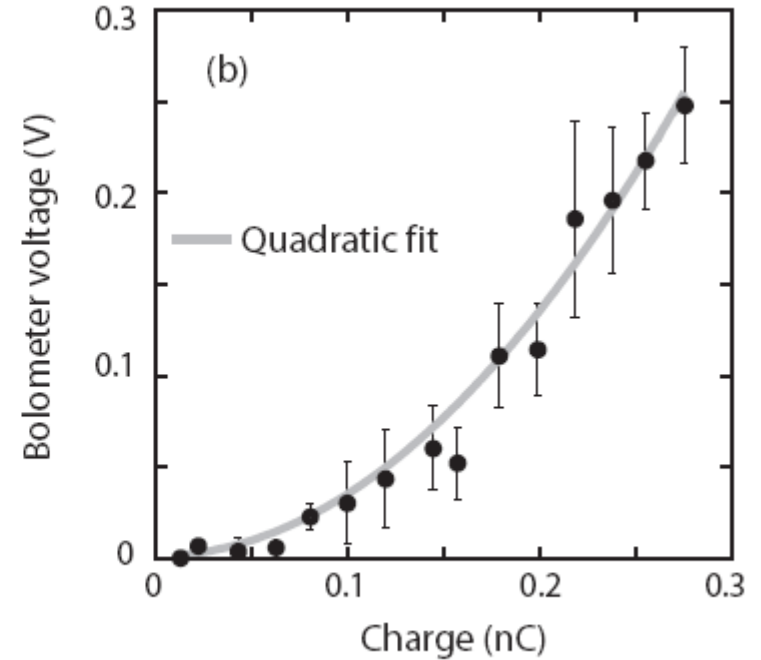
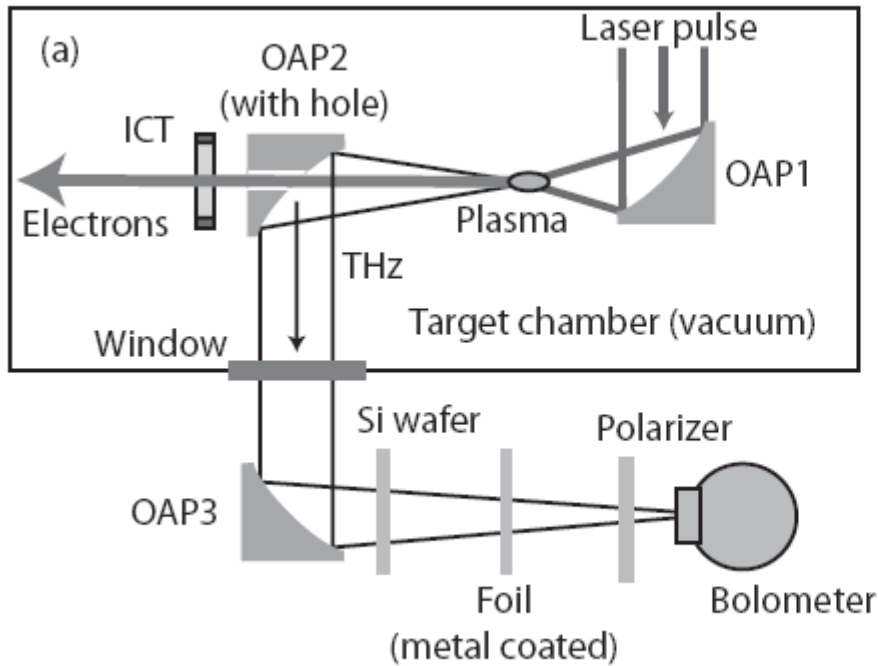


The total CTR pulse energy in units of $[\text{nJ nC}^{-2}]$, within a specific angular cone, versus transverse boundary size ρ . The radiated energy in units of $[\text{nJ}]$ is normalized to the square of the charge Q^2 (charge in units of $[\text{nC}]$). The radiation is considered to be coherent within the spectral range $\nu = 0.3 - 3$ THz. The bunch has a Boltzmann momentum distribution, with temperature $u_t = 10$. The three curves are calculated based on collection half - angles of $\theta \leq 30$ mrad (bottom curve), $\theta \leq 100$ mrad (middle curve), and $\theta \leq 200$ mrad (top curve).



$$E_{THz} \approx 4 \text{ nJ} \quad \text{for} \quad q = 1.6 \text{ nC}$$

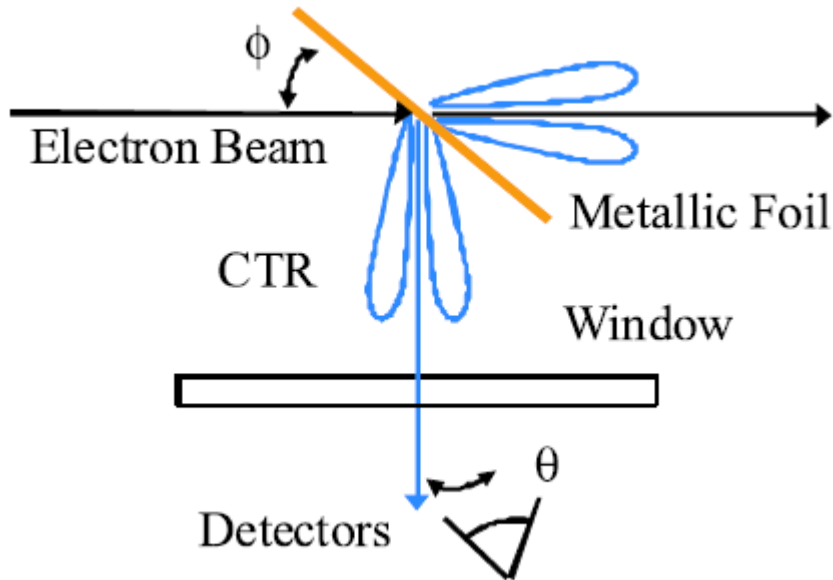
(a) Setup for measurement of the THz pulse energy. The spectral acceptance of the bolometer was 0.3–3 THz, at gain $\chi = 1000$. A thin foil reflected the THz radiation through the Rexolite window, through pieces of poly-Styrene and Teflon, and onto the bolometer. (b) Measured THz energy (~bolometer voltage) versus bunch charge. The performance of the accelerator in terms of bunch charge was varied during the data collection. The agreement between the data and a quadratic fit demonstrates the coherent nature of the radiation.



(a) Setup for measurement of the THz pulse energy. The spectral acceptance of the bolometer was 0.3 - 30 THz, at gain $\chi = 1000$. A 5 - inch - focal - length parabola (OAP2, with a) 4/5 - inch - diameter hole in the center reflected the THz radiation onto another parabola (OAP3). OAP3 focused the radiation through a silicon window, a silicon wafer, and onto the bolometer. A far - infrared polarizer was positioned in the THz beam path as well. The performance of the accelerator in terms of bunch charge was varied. (b) Measured THz energy (in terms of bolometer) voltage versus bunch charge, including a quadratic fit (solid curve).

CTR from train of bunches

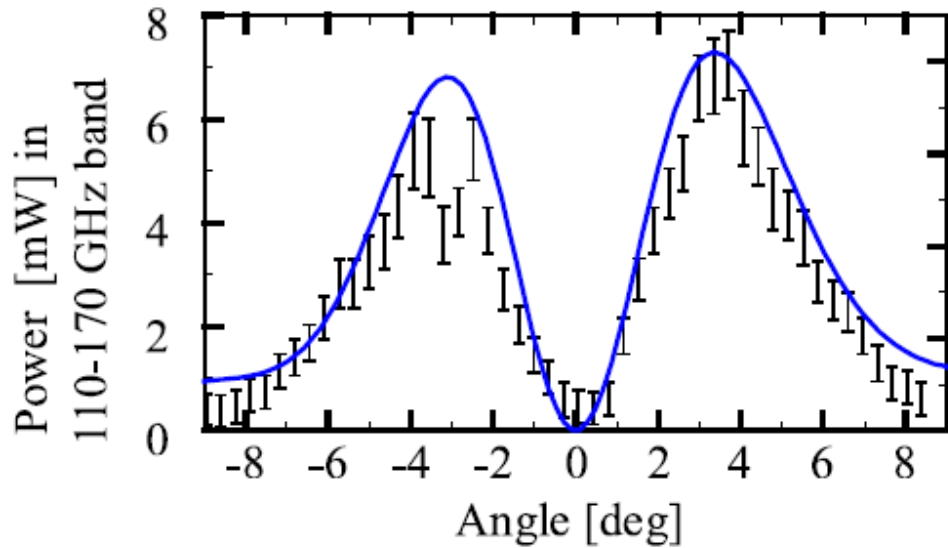
(R. A. Marsh, Phys. Rev. ST Accel. Beams 10, 082801 (2007))



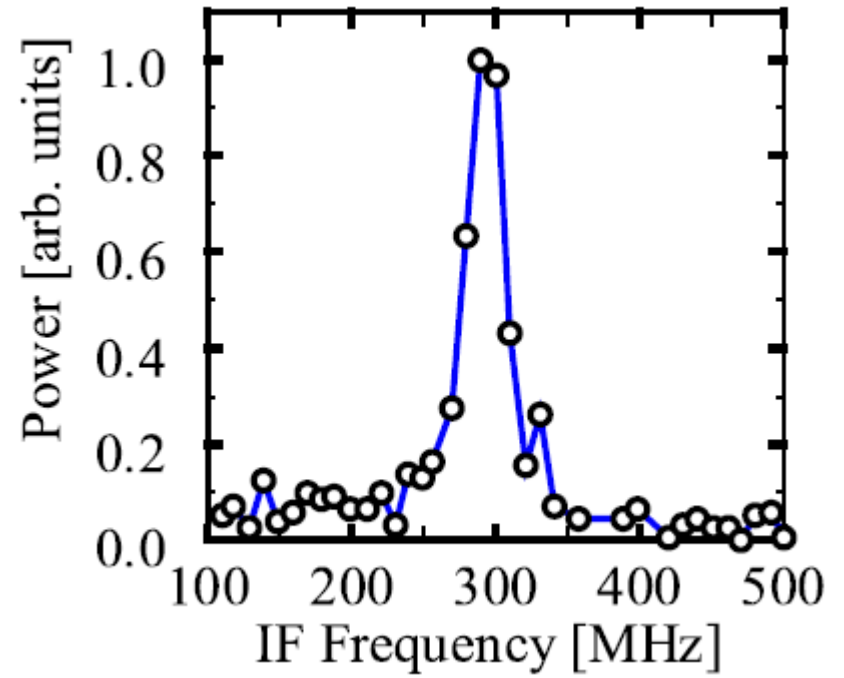
Operating parameters.

rf frequency	17.14 GHz
Beam energy	18 MeV
Bunch length	1 ps
Bunch charge	4.6 pC
Foil dimensions	5 cm×5 cm

Schematic of the experimental setup, $\phi = 45^\circ$ is the orientation angle of the foil with respect to the beam, and θ is the observation angle.



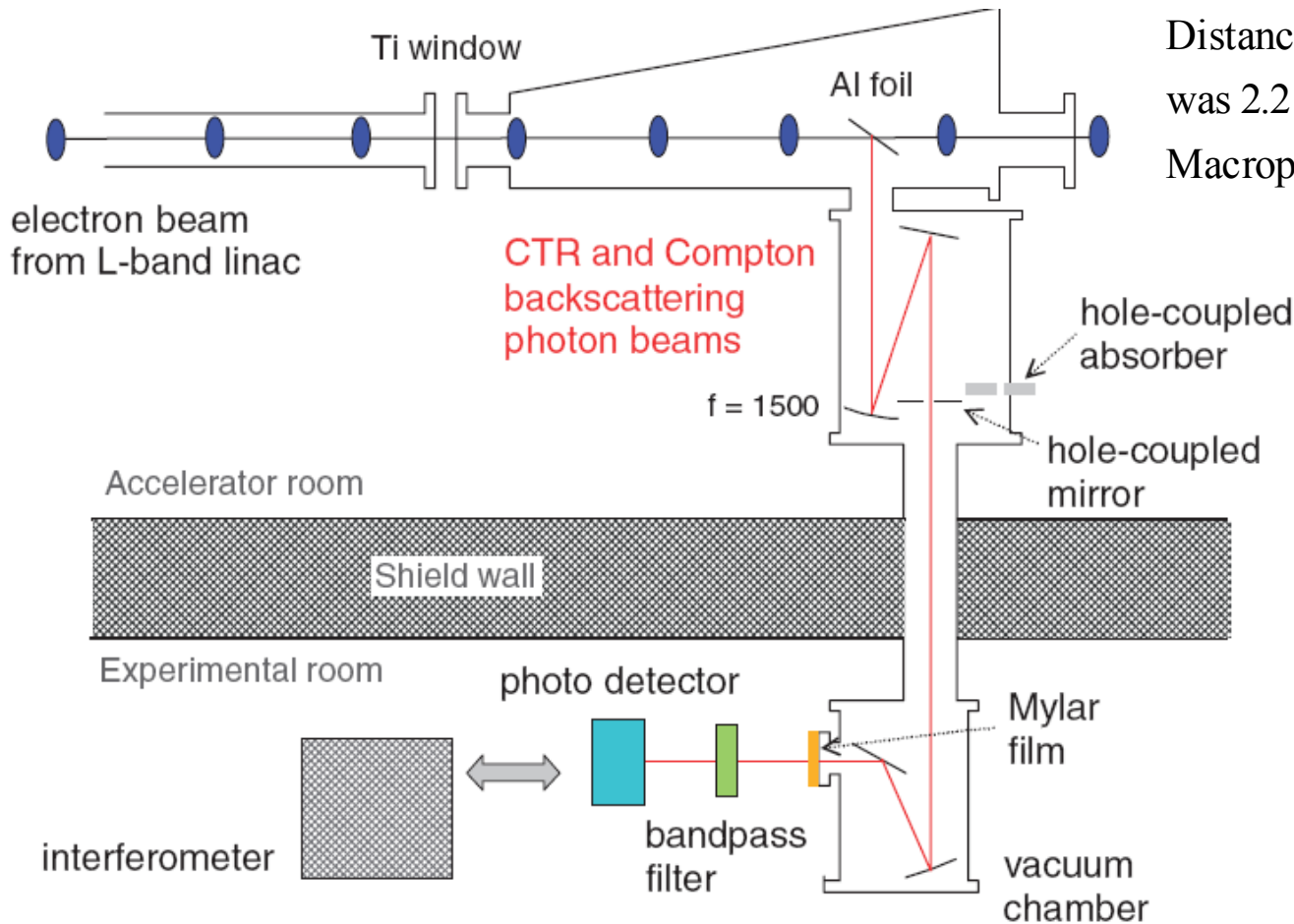
Angular distribution of CTR power measured by the diode with error bars, and theory calculations made with EFIE code, shown by the solid line. The angular error on each data point is ± 0.2 degrees.



FFT of the IF frequency from the double heterodyne receiver operating near 240 GHz, the 14th harmonic of the accelerator frequency. A narrow bandwidth of 28 MHz FWHM is observed.

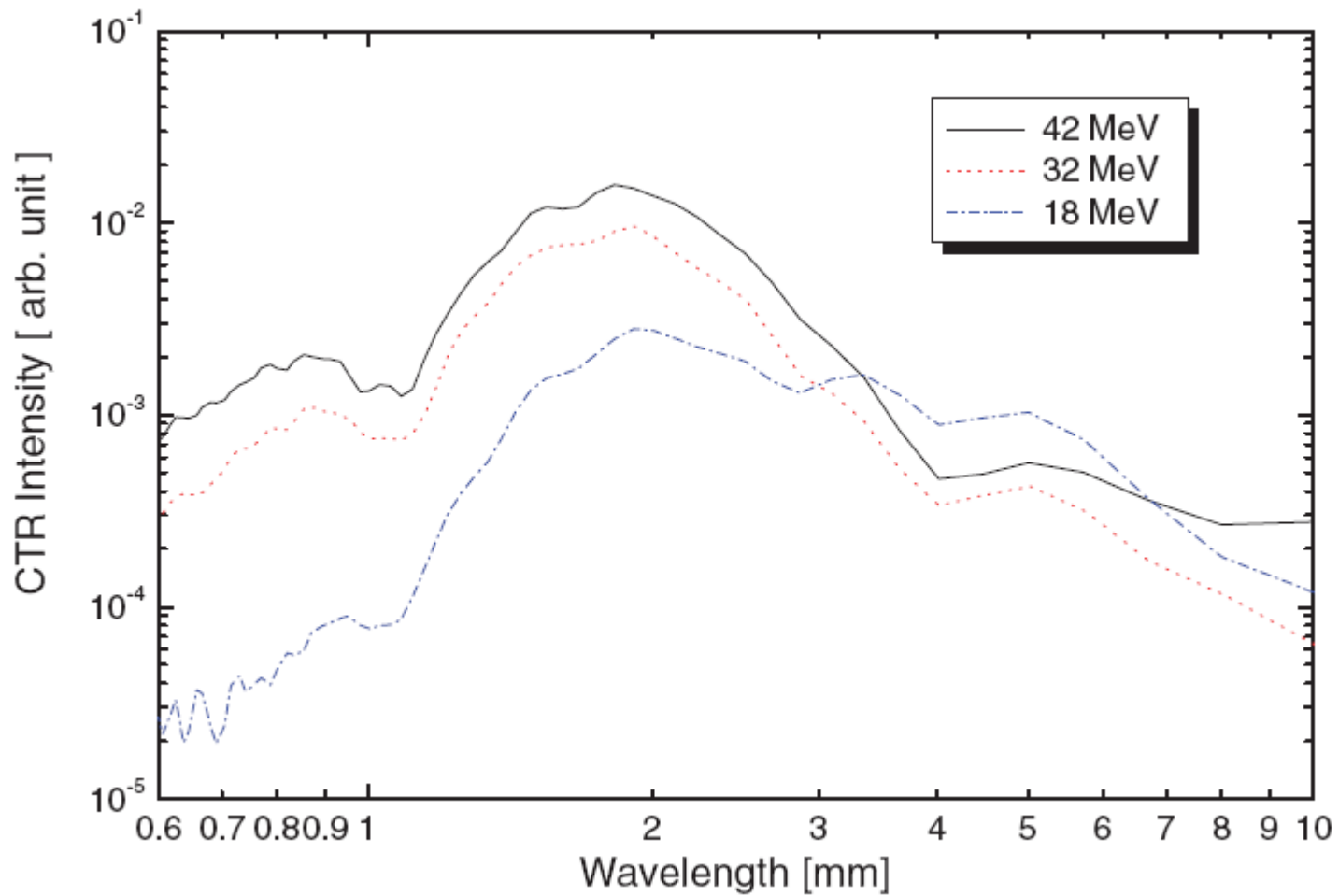
CTR

(N. Sei et al. Applied Physics Express 3 (2010) 052401)

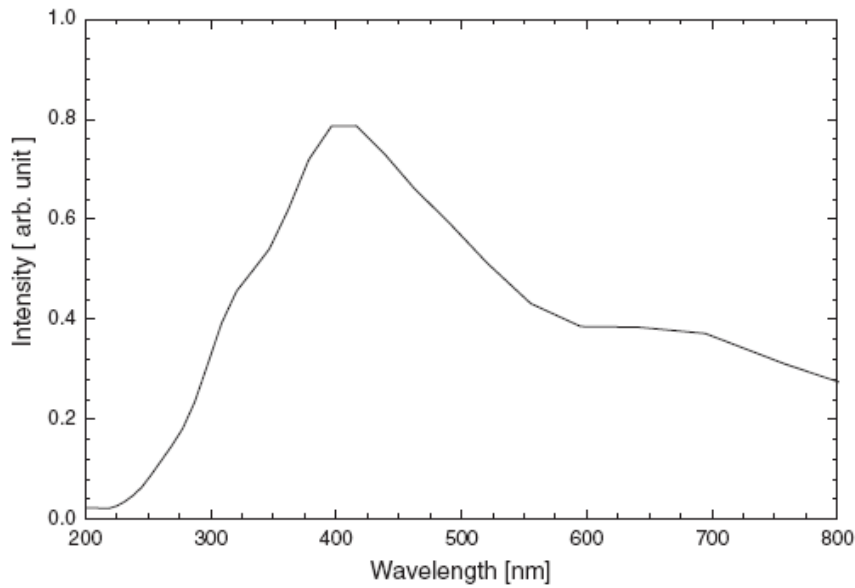


Distance between *h-c* mirror and foil was 2.2 m (round-trip time = 15 ns)
Macropulse time was 15, 33, 100 ns

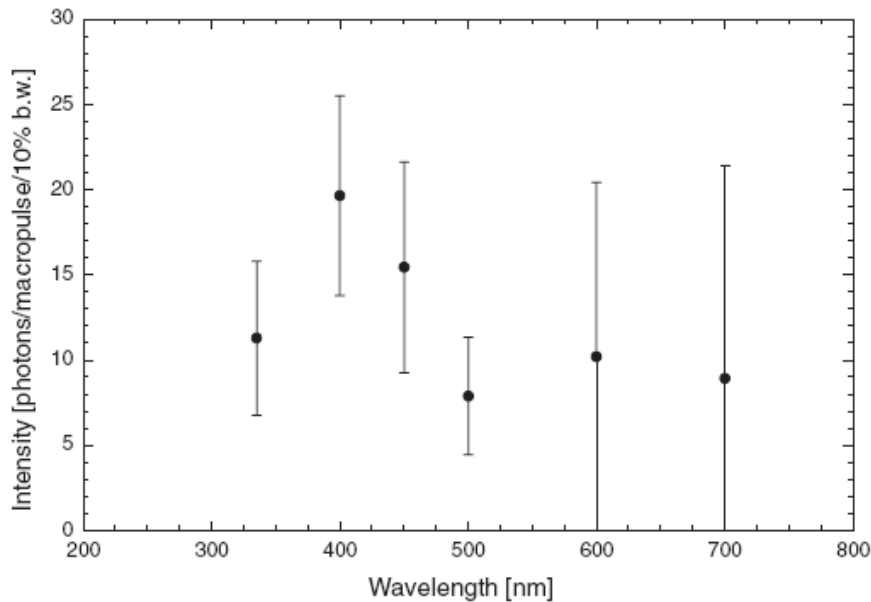
Schematic layout of the experimental setup at KURRI-LINAC.



Spectra of the coherent transition radiations measured using the interferometer at electron beam energies of 18, 32, and 42 MeV and macropulse time of 33 ns.



(a)

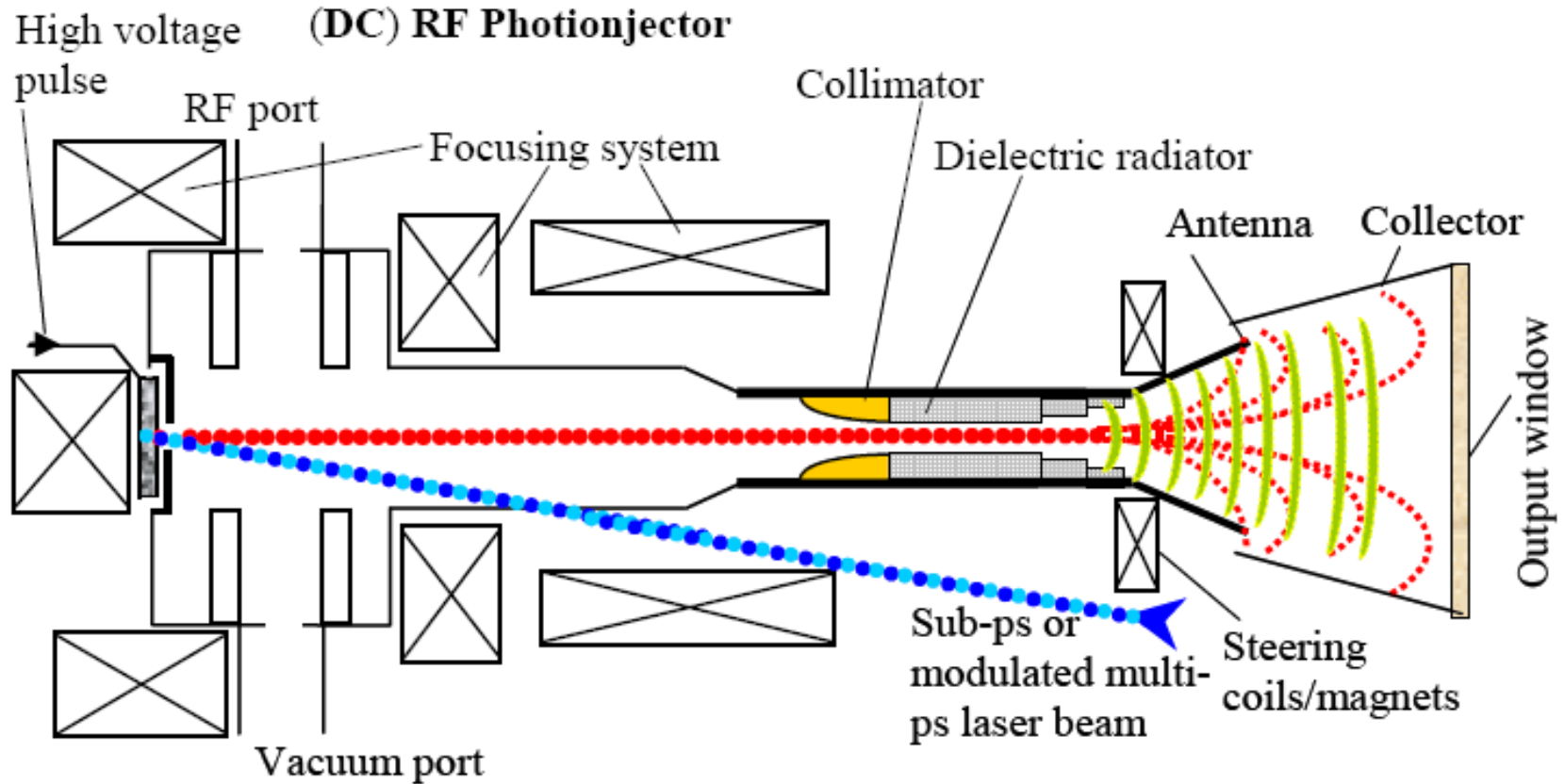


(b)

Spectrum of the Compton backscattered photons calculated using the CTR spectrum (a), and spectrum of Compton backscattered photons measured using the light sensor module (b). The central wavelengths of the bandpass filters are 340, 400, 450, 500, 600, and 700 nm. The intensity in (b) is shown in units of photon number per macropulse for a bandwidth of 10%.

Cherenkov radiation

(A. V. Smirnov, In: Photonics Research Development,
Ed. Viktor P. Nilsson, pp. 247-269, Nova Science Publishers, Inc., 2008)

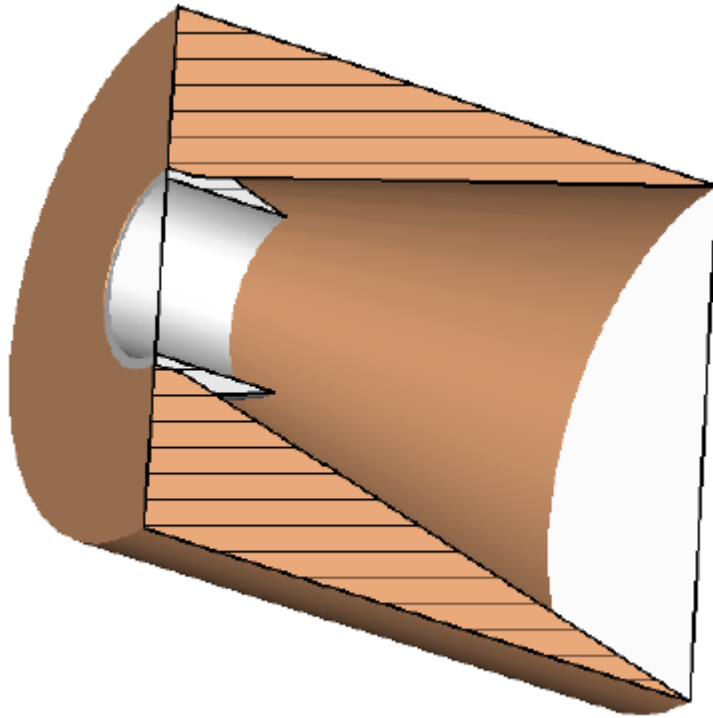


Schematic layout of sub-mm, high-peak power, dielectric-based generator based on 2-cell, pulse RF or DC-RF electron gun.

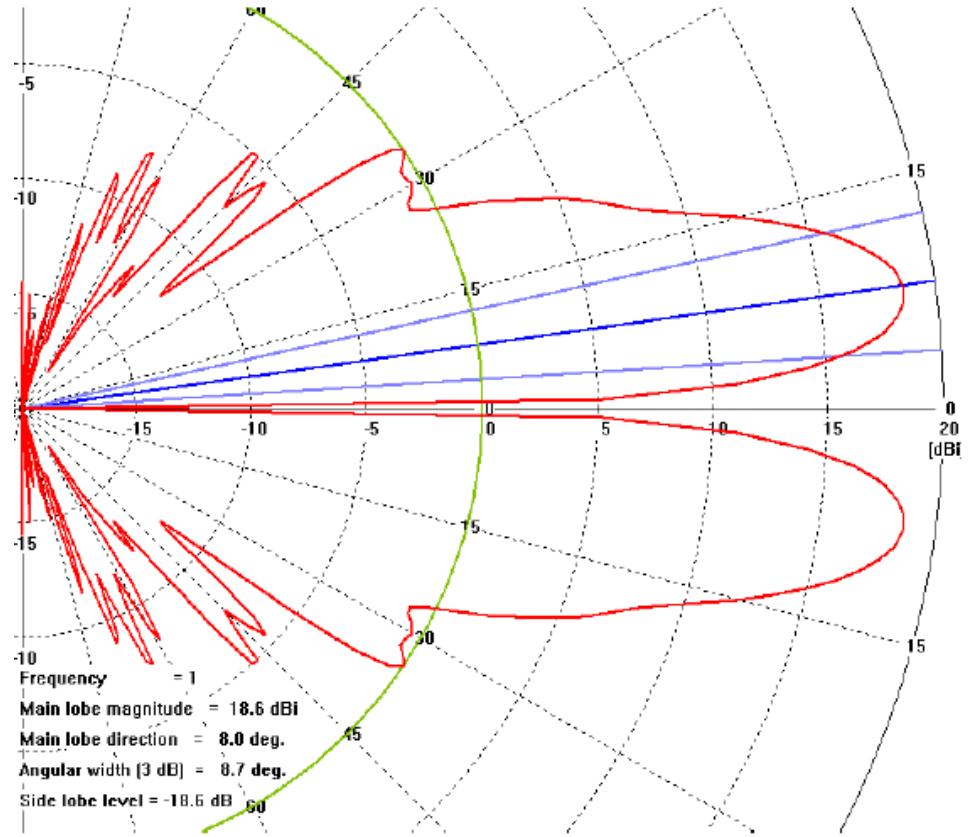
$$Q \sim 150 \text{ pC}, \quad \tau_B \sim 50 \text{ fs}$$

TM01 mode parameters for a capillary channel at 0.95-0.97 THz resonant frequency and different coating materials

Material (cross-section)	Dielectric constant ϵ	Beam aperture radius a, μm	Dielectric thickness d, μm	Beam Kinetic energy W, MeV	Shunt impedance/Q R/Q, kOhm/m	Group velocity β_{gr}	Q-factor estimation
Teflon (circular)	2.08	300	31	3.2	14.7	0.82	1900
		520	26	2	1.07	0.89	2440
Barium tetratitanate	37	300	30	0.5	27.7	0.127	587
Sapphire	11.5	300	14	4	18.9	0.76	1176
Fused quartz or silica	3.78	336	18.8	4	12.4	0.83	2070
Diamond (quadratic)	5.7	336	16	4	12.7	0.821	1834
		300			8	0.829	1700

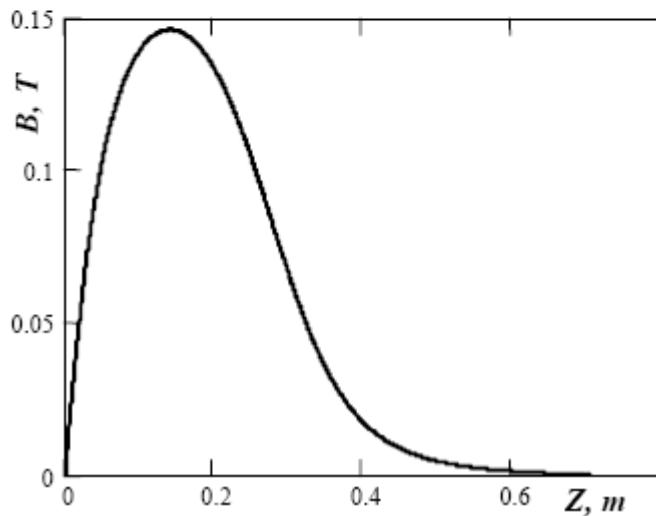
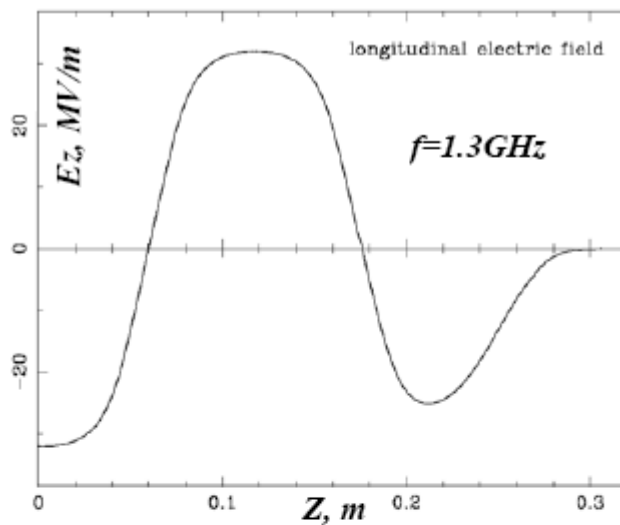


a)

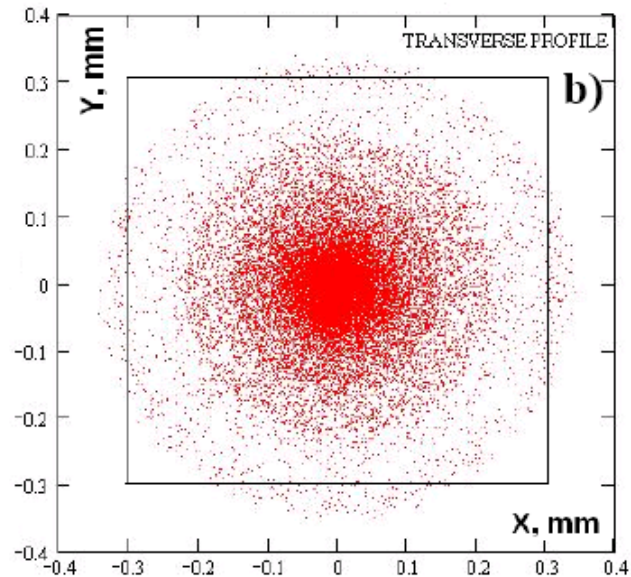
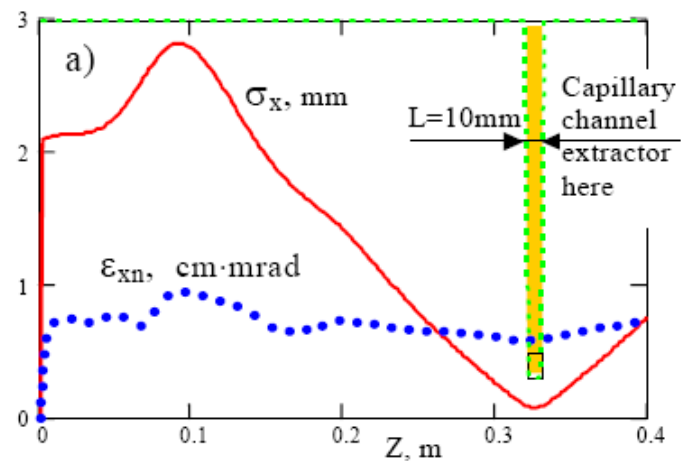


b)

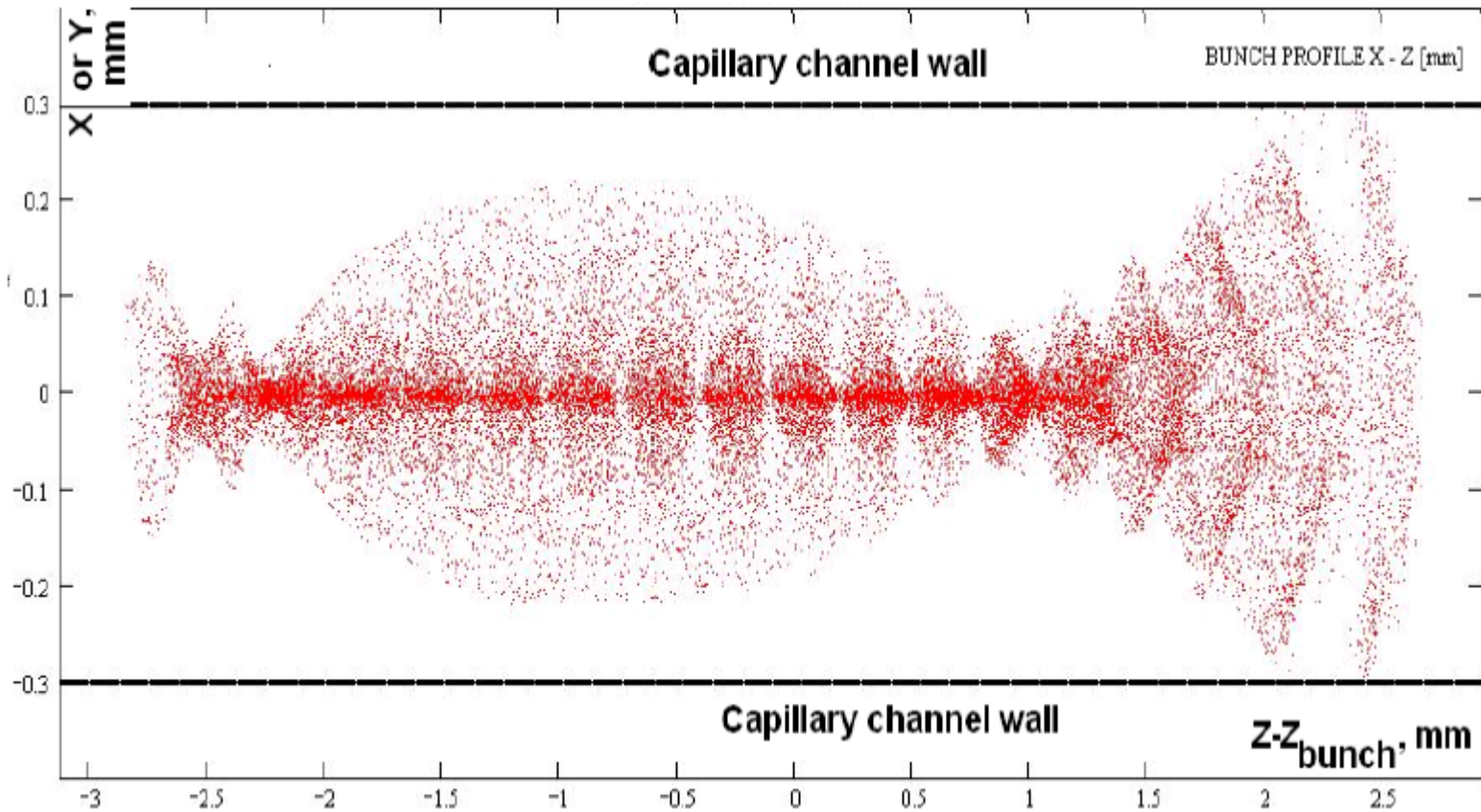
Antenna supplied by internal dielectric lens (a) and its far-field pattern (b).



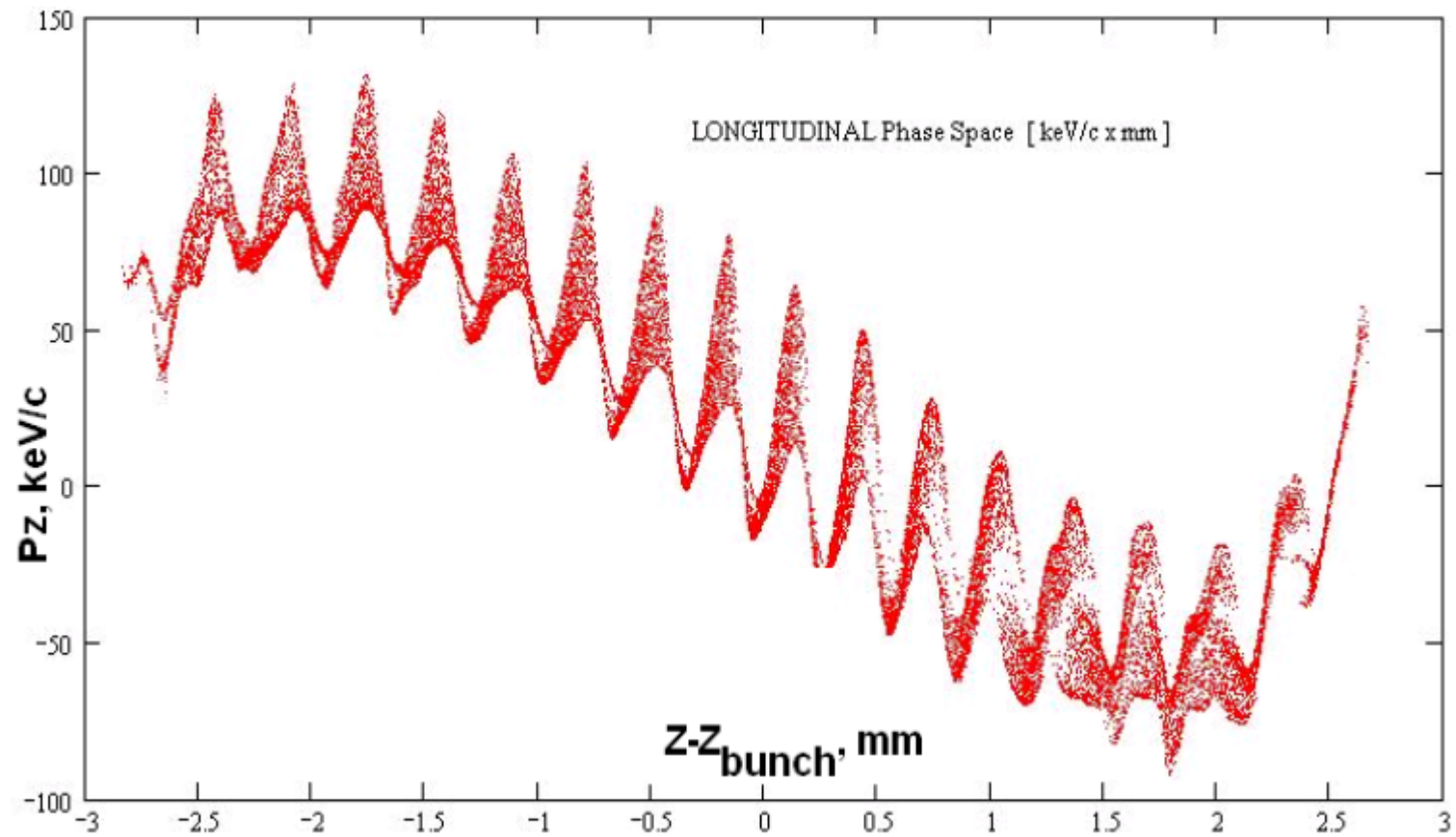
Longitudinal RF electric and magnetostatic field profiles used in simulations of 2-cell RF photoelectron gun.



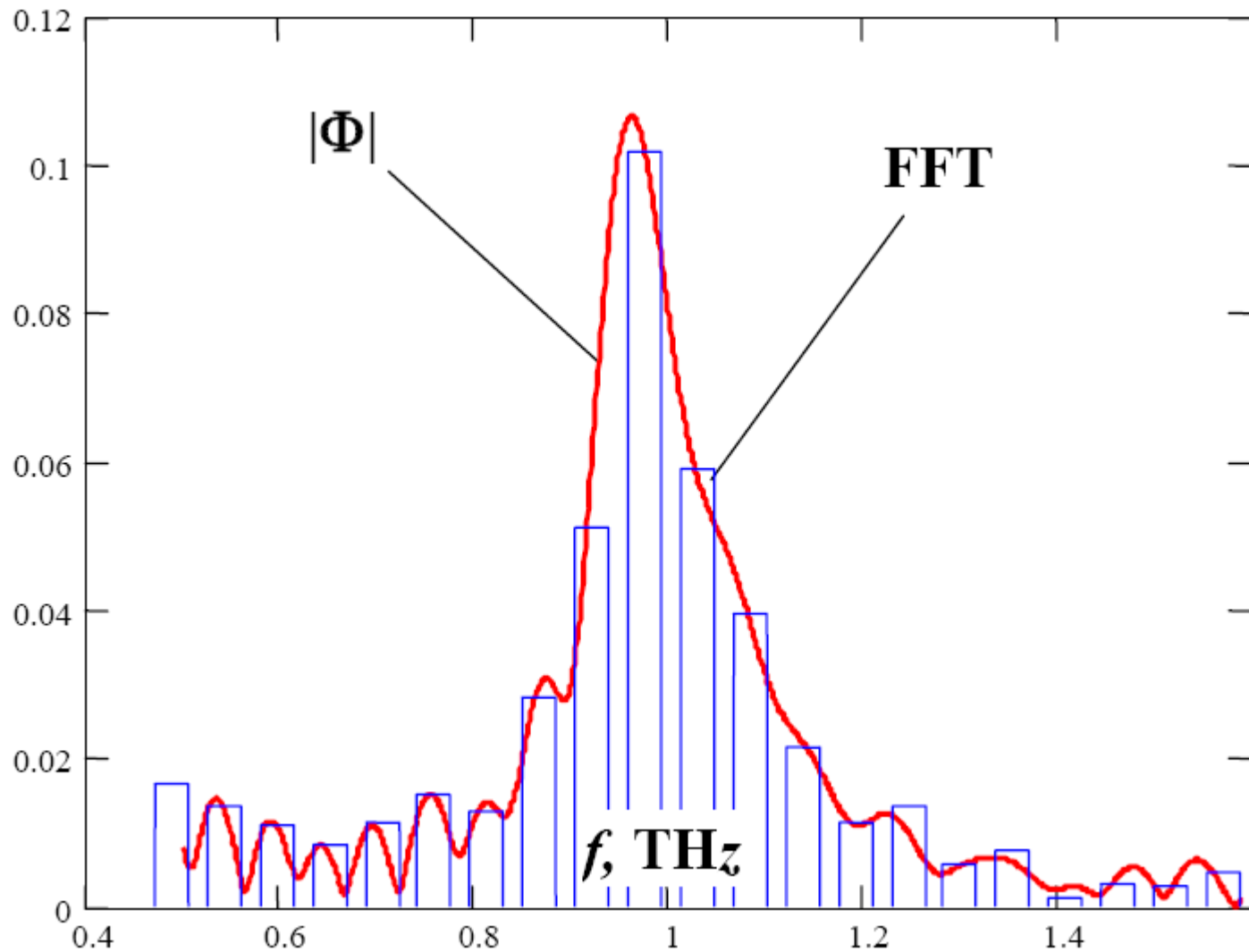
Beam rms horizontal (or vertical) dimension (solid curve) and normalized, transversally uncorrelated emittance (dotted line) plotted as a function of the distance from the cathode (a), and beam transverse profile at the waist (b). Laser pulse length is 26 ps, bunch charge is 2nC, maximum RF electric field in the accelerating cavity is $E_{z\text{max}}=32 \text{ MV/m}$, $B_{z\text{max}}=1.46 \text{ kGs}$, and beam kinetic energy is 4 MeV.



Beam X-Z or Y-Z transverse profile inside the capillary channel. Modulation is produced with two-wave beating having 1.555ps period of intensity at the cathode. Laser flat-top pulse length is 26ps, the capillary channel center is positioned at $z=0.326\text{m}$ from the cathode.



Longitudinal phase space of the microbunched beam near its waist in the capillary channel.



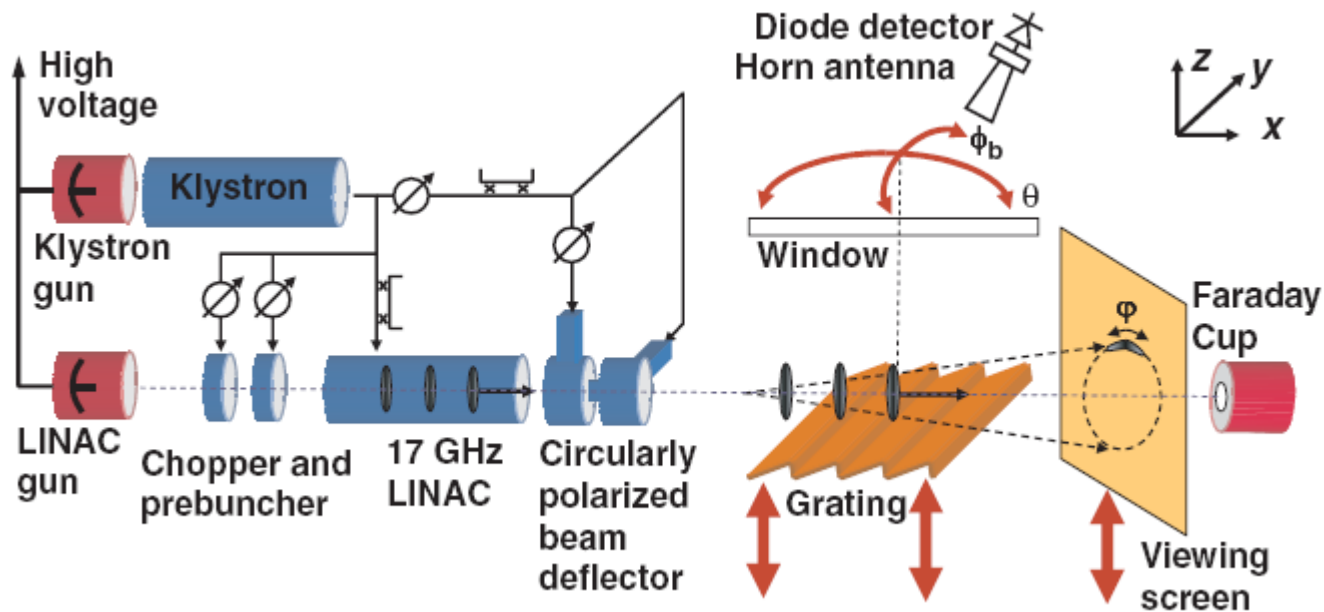
Fourier transform of the charge distribution along the bunch (bars) and formfactor as a function of frequency at $z=0.326\text{m}$.

$$W_{\text{CHR}} \sim \mu\text{J}/\text{bunch}, \quad \Delta\omega/\omega \sim 10\%$$

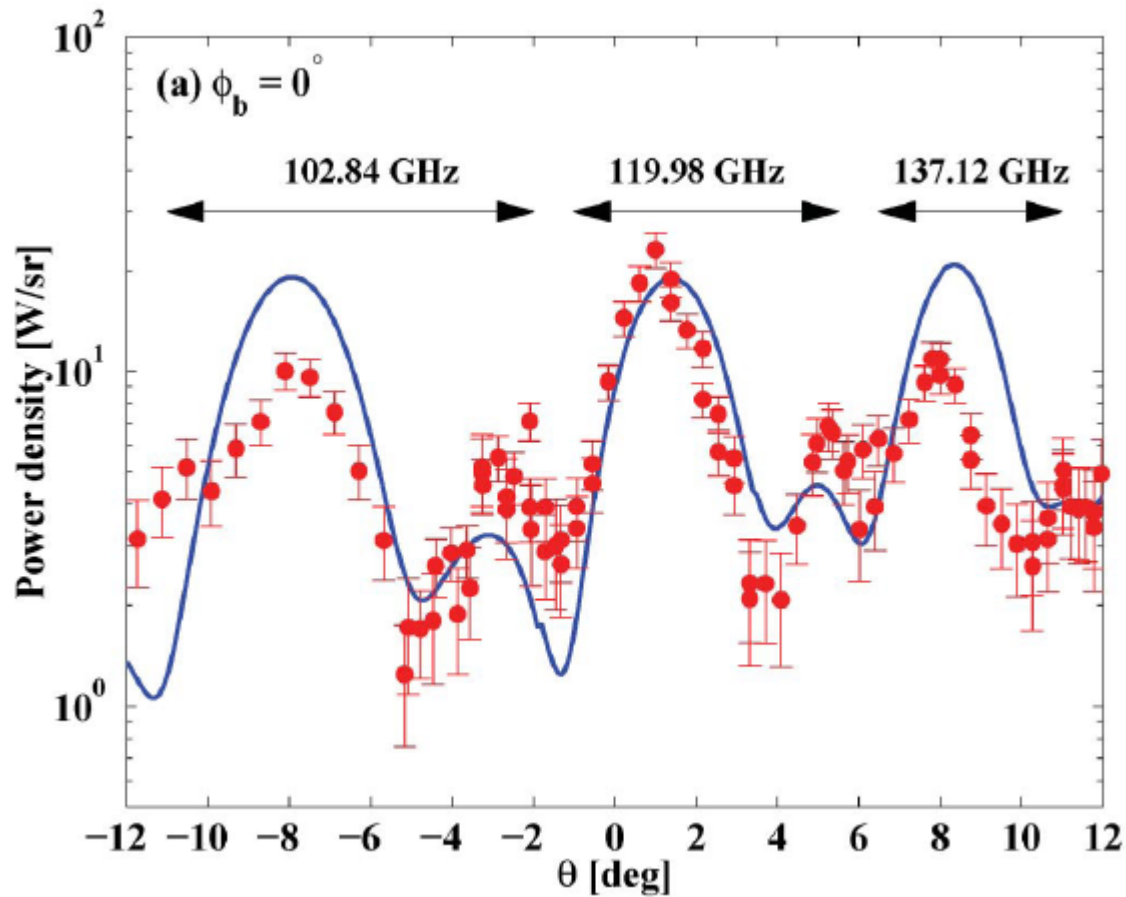
Smith – Purcell Radiation

(M. Kesar et al., Phys. Rev. ST Accel. Beams 9, 022801 (2006))

A 50 ns long train of 170 m electron bunches was produced by a 15 MeV, 17 GHz accelerator with 80 mA of average current.



SPR experimental setup (not to scale) including the klystron, linac, deflecting cavities and screen, and the grating.



Measured power density in W / sr (dots with error bars). The measurement is compared to the first - order radiated power density by the EFIE model (solid line). The power is plotted versus θ when $\Phi_b = 0^\circ$ (a).

Summary

- A lot of applications of THz beams
- A direct conversion from laser flash to THz radiation is not so effective
- Advantages of generation of THz radiation from short electron bunches (via different emission mechanisms):
 - higher efficiency (in comparison with direct laser energy transformation)
 - directivity
 - large radiation angle (up to 90°)
 - possibility to obtain monochromatic THz beam using Smith Purcell mechanism and from of bunches

Thanks for your attention